IEEE Access
Multidisciplinary : Rapid Review : Open Access Journal

Received 6 December 2023, accepted 21 December 2023, date of publication 26 December 2023, date of current version 4 January 2024.

Digital Object Identifier 10.1109/ACCESS.2023.3347587

RESEARCH ARTICLE

Improved PSO With Visit Table and Multiple Direction Search Strategies for Skin Cancer Image Segmentation

YAGMUR OLMEZ[1], GONCA OZMEN KOCA[1], ABDULKADIR SENGÜR[2], U. RANJENDRA ACHARYA[3], (Senior Member, IEEE), AND HASAN MIR[4], (Senior Member, IEEE)

[1]Department of Mechatronics Engineering, Firat University, 23119 Elazig, Turkey
[2]Department of Electrical and Electronics Engineering, Firat University, 23119 Elazig, Turkey
[3]School of Mathematics, Physics and Computing, University of Southern Queensland, Springfield Central, QLD 4300, Australia
[4]Department of Electrical Engineering, American University of Sharjah, Sharjah, United Arab Emirates

Corresponding author: Abdulkadir Sengür (ksengur@firat.edu.tr)

ABSTRACT Automated screening is employed to assist skin specialists in accurately detecting skin lesions at an early stage. Multilevel thresholding is a widely popular and efficient technique for enhancing the classification of skin cancer images. This paper proposes improved PSO with a novel visit table and multiple directions search strategies to develop the performance of the multilevel thresholding. A visit table strategy has been developed that prevents unnecessary searches of the original particle swarm optimization (PSO) algorithm by allowing the discovery of new points by making fewer visits to frequently visited points and their neighbors. Besides, a multiple directions search strategy has been introduced for the PSO to increase the diversity of the population and overcome the stuck at the local optimum by enhancing exploration ability. The qualitative, quantitative, and scalability analyzes of the improved PSO (IPSO) method were carried out on 50 benchmark functions and the highest performance was achieved with the proposed method in most of these functions. Secondly, a multilevel image segmentation application is presented on skin cancer images using two-dimensional (2D) non-local means histograms, improved PSO and Renyi's entropy. In this work, the ISIC 2017 skin cancer image dataset is used for segmentation application and various performance evaluation metrics are used. The obtained results are compared with seven state-of-the-art approaches to show the efficiency of the proposed approach. It can be noted from the obtained results that, the proposed method outperforms the compared method based on the average of evaluation metrics for all skin cancer images. The best results in SSIM value of 0.8285, FSIM value of 0.7332, and PSNR value of 19.0576 are achieved by using the proposed method in skin cancer image segmentation. Hence, our proposed method is ready to be tested with huge databases and can aid skin specialists in making an accurate diagnosis.

INDEX TERMS Multilevel thresholding, multiple directions search strategy, PSO, skin cancer, visit table strategy.

ACRONYMS

Parameters	Definitions.
X	Positions of the particles.
V	Velocities of the particles.
w	Momentum inertia.
C_1, C_2	Acceleration Factors.
Npop	Number of the Particles.
Max_{iter}	Max. Number of the iteration.
iter	Current iteration.
d	Dimension of the problem.
R_1, R_2	Random numbers with uniform distributions.

The associate editor coordinating the review of this manuscript and approving it for publication was Andrea Bottino.

P_{best}	Local Optimum.
G_{best}	Global Optimum.
F_{Pbest}	Local best fitness value.
F_{Gbest}	Global best fitness value.
Up	Upper bound of the particles.
Low	Lower bound of the particles.
IPSO	Improved Particle Swarm Optimization.

I. INTRODUCTION

Skin cancer (SC) is a serious and common disease that can affect anyone, regardless of race, gender, or age. Malignant is one of the skin cancer types and is considered as most prevalent and deadly type [1]. Early diagnosis of malignant melanoma can significantly reduce the mortality rate and reduce the costs of the treatment. This can be achieved by using the proposed approaches more accurately and effectively to determine cancer types and by improving the performance of these approaches. This encourages researchers to develop new techniques and enhance the performances of the existing ones. Image segmentation is one of the most critical steps of image processing in early diagnosis of cancer type, medical applications, surgical applications, etc.

Metaheuristic algorithms are widely used in many fields to obtain the most effective solutions for various problems. Some of these fields are; image processing [2], [3], control techniques [4], [5], deep learning models [6], [7], machine learning algorithms [8], optimal filter design [9], text clustering [10], feature selection [11], etc. Segmentation is the first and most important step in image processing [12]. Thresholding is one of the simplest techniques used in image segmentation. It is classified as bi-level and multilevel thresholding. In image segmentation, metaheuristic algorithms are commonly applied for multilevel thresholding. The computational cost of using traditional thresholding segmentation approaches rises exponentially with the number of thresholding levels, which limits their applicability to a restricted set of thresholding levels. The authors are motivated to utilize metaheuristics-based multilevel thresholding segmentation methods as an alternative to the conventional techniques of this difficulty. In addition, the multi-level thresholding segmentation problem is a reasonable application for performance evaluations of metaheuristic approaches, as increasing the number of thresholds increases complexity. From this point of view, the multilevel thresholding segmentation problem is one of the most common problems that many researchers use after the test functions to determine the effectiveness of their proposed metaheuristic algorithms.

Many multilevel thresholding approaches based on metaheuristics have recently been developed that segment images of different types into various applications. Some existing studies developed on multilevel thresholding segmentation are summarized in Table 1 using different types of images.

An improved version of the golden jackal optimization algorithm has been employed to solve the multilevel thresholding problem using Otsu's maximum variance [1]. An adaptive multilevel thresholding method based chaotically enhanced Rao algorithm has been proposed in [12]. It is shown that the proposed method has better segmentation results compared to the other multilevel thresholding methods on most of the 13 evaluation metrics. Kurban et al. has performed a multi-level color thresholding segmentation using the six state of art metaheuristic algorithms, which are equilibrium optimization algorithm, slime mould optimizer, turbulent flow of water-based optimization algorithm, henry gas solubility optimization, marine predator's optimization algorithm, and political optimization [13]. The results have been assessed in terms of reference image-based metrics, and no-reference image quality metrics. A hybridized optimization algorithm has been proposed for the multilevel thresholding of satellite images [14]. The results have shown that the proposed method outperformed other techniques. Researchers have realized the multilevel thresholding segmentation of skin cancer by using metaheuristic algorithms [1], [15], [16]. The segmented image is generally utilized in the post-processing step for better evaluation. A modified differential evolution optimization algorithm has been proposed by Ren et al. [15]. Zhu et al. have improved an efficient version of the Whale Optimization Algorithm with a chaotic random mutation strategy and Levy operator [16]. In addition to skin cancer images, metaheuristic methods are used in the segmentation of various medical images. Medical image segmentation has been performed using 2D and 3D medical images from different modalities, such as MRI, CT, and X-ray, by Hosny et al. [17]. Jena et al. has proposed a novel metaheuristic algorithm called attacking Manta Ray foraging optimization [18]. They have also proposed a maximum 3D Tsallis entropy as an objective function for multilevel thresholding segmentation of MR images. A modified slime mould algorithm has been proposed for the multilevel thresholding segmentation [19]. The experimental studies have shown that the proposed method is quietly successful in the segmentation of Lupus Nephritis images.

The existing segmentation studies presented above were performed on grayscale and color images. This study aims to advance grayscale image segmentation by enhancing the PSO method. The study aims to show the effectiveness of the proposed method with 50 different modalities, benchmark functions, and multilevel thresholding. Multilevel thresholding is suitable to demonstrate the effectiveness of metaheuristic methods due to its complexity, which increases as the segmentation level increases. Secondly, it is aimed at improving the performance of skin cancer segmentation. This study proposes an improved PSO with a multiple directions search and the visit table strategy optimization method to perform multilevel thresholding on skin cancer images. The proposed method, which is an efficient and improved version of the original PSO, is developed to solve a few drawbacks of the original PSO method. Firstly, it is aimed to prevent

TABLE 1. Summary of comparison with State-of-the-Art techniques developed for skin lesion segmentation.

Authors	Optimization method	Thresholding Method	Dataset	Obtained results
Houssein et al. [1]	Improved golden jackal optimization algorithm	• Otsu's method	• Skin cancer images	The method effectively resolves the skin cancer segmentation problem.
Yang et al. [2]	Enhanced differential evolution	• Kapur's entropy	• Breast cancer images • 30 Benchmark functions	The suggested approach for determining thresholds expedites the convergence process and mitigates the issue of premature convergence.
Olmez et al. [12]	Chaotically-enhanced Rao algorithm	• Otsu's method	• Berkeley Benchmark	It outperformed the compared methods in terms most of image quality metrics.
Kurban et al. [13]	Marine predator and turbulent flow of water-based algorithms	• Kapur's entropy, • Otsu's method	• Color aerial images	It outperformed the other six algorithms in terms of five image quality metrics and CPU time consumption.
Swain et al. [14]	Equilibrium-cuckoo search optimizer	• Differential exponential entropy	• Color satellite images	The performance was enhanced by including more edge information and improving search space exploration.
Ren et al. [15]	Modified differential evolution	• Kapur's entropy	• Breast cancer • Skin cancer images	It outperformed many competitors who provided similar services.
Wei et al. [16]	Boosting whale optimizer	• Kapur's entropy	• Skin cancer images	The method outperformed other WOA variants.
Hosny et al. [17]	Hybrid Coronavirus Algorithm	• Otsu's method, • Kapur's entropy	• 2D and 3D medical images	Better quality solutions were acquired for 2D and volumetric medical image segmentation.
Jena et al. [18]	Attacking Manta-Ray foraging optimization	• 3D Tsallis entropy	• Brain MR images • 27 Benchmark functions	The method outperformed 1D and 2D Tsallis entropy-based methods.
Chen et al. [19]	Slime mould algorithm with bee foraging mechanism	• Kapur's entropy	• Lupus nephritis images	It improved the performance of the multilevel thresholding.
Kumar et al. [20]	Efficient cuckoo search algorithm	• Recursive minimum cross-entropy	• Crop images	Results are expressed in terms of SSIM, FSIM, PSNR, MSE, and CPU time.
Wang et al. [21]	Improved whale optimization	• Otsu's method, • Kapur's entropy	• 10 benchmark images	It has better performance in terms of convergence and segmentation quality.
Proposed Method	Improved particle swarm optimization	• Renyi's entropy	• Skin cancer images • 50 Benchmark functions	It outperformed the other seven algorithms in SSIM, FSIM, PSNR, CPU time, and a set of statistical tests.

unnecessary searches by adding a visit table strategy to the algorithm. Secondly, a new movement equation is presented to avoid stacking into the local optimum. In the experiments, the method was applied to two different datasets. The first experiments were performed on 50 benchmark problems that have different properties. In addition to quantitative and qualitative analysis of the proposed method, the scalability analysis was also performed. The experimental results were compared with seven other metaheuristic methods: AOA (Arithmetic Optimization Algorithm), GWO (Grey Wolf Optimization), MFO (Moth Flame Optimization), WOA (Whale Optimization Algorithm), MVO (Multi-Verse Optimization), TLBO (Teaching Learning Based Optimization), and original PSO (Particle Swarm Optimization). The outcomes showed that for the majority of the benchmark functions, the improved PSO method works better than the original PSO and other state-of-art methods. Secondly, a multilevel thresholding image segmentation method based developed optimization algorithm was proposed using Renyi's entropy and non-local means 2d histogram. The experimental results of segmentation demonstrate that the proposed approach works better than other algorithms in terms of the SSIM (Structured Similarity Index), FSIM (Feature Similarity Index), and PSNR (Peak Signal to Noise Ratio) image quality metrics.

The main contributions of this paper are summarized as follows:

- ➢ Improved PSO (IPSO) with visit table and multiple directions search strategies is introduced to address the issue of multilevel thresholding segmentation.
- ➢ The proposed optimization method is developed based on the visit table strategy to prevent unnecessary searches and increase diversity. By adding a visiting table and a new position updating equation to the original PSO, exploration, and exploitation steps are improved and prevented from getting stuck in the local optimum.
- ➢ A multilevel segmentation framework is presented on skin cancer images using 2d non-local means histogram and Renyi's entropy as an objective function.
- ➢ The performance of the proposed method is assessed with a different threshold level.
- ➢ The proposed method is compared with several state of art methods.
- ➢ The effectiveness of the proposed optimization method is validated with qualitative analysis, quantitative analysis, and scalability analysis.

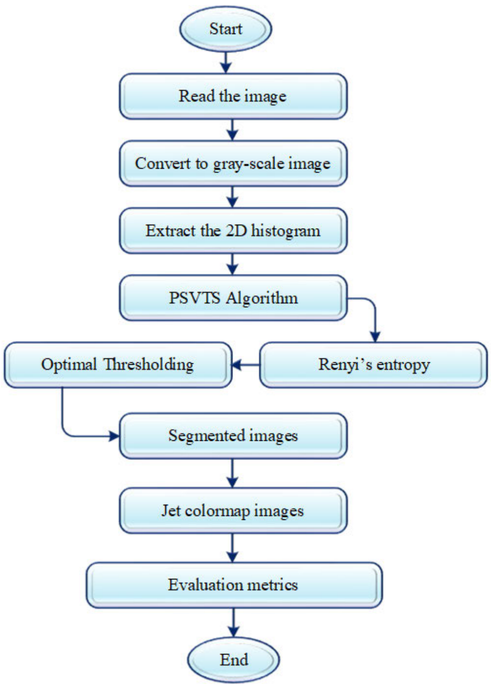

FIGURE 1. **Flowchart of the image segmentation method.**

- ➢ The efficiency of the segmentation technique is validated using PSNR, FSIM, and SSIM evaluation indexes.
- ➢ The suggested method can be applied to image Furthermore, various developed visit table strategies can also be applied to improve the performance of the metaheuristic algorithms.

The rest of the paper is organized as follows. In Section II, the proposed multilevel thresholding image segmentation method and improved PSO algorithm are explained. Experimental studies and results obtained are presented in Section III. Finally, the conclusion and future work are given in Section IV.

II. MATERIALS AND METHODS

This section provides a detailed description of the multilevel thresholding image segmentation problem and the proposed image segmentation framework based on improved particle swarm optimization with a visit table and multiple directions search strategies.

A. DESCRIPTION OF MULTILEVEL IMAGE SEGMENTATION PROBLEM

A multilevel thresholding method is developed to enhance the segmentation of pathological skin cancer images. The developed method is based on a non-local means histogram which utilizes the redundant information in the image and keeps the most detailed elements of the image. It also uses information on the gray-scale images and spatial correlation of the pixels. Since the computational cost of using traditional thresholding segmentation approaches rises exponentially with the number of thresholding levels, an efficient multilevel thresholding method is integrated into the segmentation method. Renyi's entropy is used as the objective function, which calculates the entropy difference between the object and the background and its absolute value. The optimal thresholding values are found where the entropy is maximum. Renyi's entropy is maximized as $T^* = \arg maxH_M$. Hereby, the multilevel thresholding image segmentation method based on the PSVTS optimization algorithm nonlocal means 2D histogram and Renyi's entropy is proposed. The flowchart of the segmentation method is presented in Figure 1 in detail. Firstly, the original skin image is read and converted into the gray-scale image. The 2D histogram is constructed by a nonlocal means filter. The histogram is given to the proposed optimization method as input. The optimal thresholding values are obtained in the optimization method where Renyi's entropy is maximum. The original images are segmented with the obtained optimal thresholding values. The segmented images are assessed with a set of image quality evaluation metrics.

B. ORIGINAL PSO

Particle swarm optimization is one of the most common and basic optimization techniques inspired by the behavior of animals living in herds. There are 2 main parameters of the PSO technique, which are pbest and gbest. The best position of the particle is defined as pbest and the swarm's best position is defined as gbest. In each iteration, the positions of the particles are updated according to pbest and gbest values [22]. The updating equations of the positions can be given as:

$$v_{ij}(k+1) = v_{ij}(k) + C_1\, rand_1 \left(P_{best,ij}(k) - x_{ij}(k)\right) + C_2\, rand_2 (g_{best,ij}(k) - x_{ij}(k)) \quad (1)$$

$$x_{ij}(k+1) = x_{ij}(k)) + v_{ij}(k+1) \quad (2)$$

where, $v_{ij}(k)$ and $v_{ij}(k+1)$ represent the current and the next velocities of the particles, respectively. C_1 and C_2 are acceleration coefficients. $rand_1$ and $rand_2$ are the random vectors. $x_{ij}(k)$ and $x_{ij}(k+1)$ denote the current and the next positions of the particles, respectively.

C. IMPROVED PSO

This section introduces details of the proposed improved PSO (IPSO) algorithm in four subsections inspiration, mathematical model, procedure, and the computational complexity of the algorithm. The pseudocode of the proposed method is given in Algorithm 1. The relevant sections are explained in detail as the following.

1) INSPIRATION

The main purpose of the optimization problem is to acquire the optimum solution in the defined search space for the problem as soon as possible. Although the PSO algorithm is one of the oldest developed algorithms, it is still one of the most frequently used methods today due to its simple structure and easy-to-understand and applied method. However,

Algorithm 1 Pseudocode of the Improved PSO

1) Initialize the velocities, population, pBest, gBest, visit table, direct vector
2) Calculate the fitness values of each particle
3) Determine gBest and pBest
4) for k=1:iter
   a) for i=1:Npop
   b) Update Direct Vector
   c) Update Target Index
   d) if rand<Threshold
      i) Update velocity and position using Eqs. 6-7.
      ii) Calculate newF
      iii) Update VisitTable
      iv) If newF>Fi
         (1) Fi = newF
      v) Endif
   e) Else
      i) Update velocity and position using Eqs.8-9.
      ii) Update VisitTable
      iii) Calculate newF
      iv) If newF<Fi
         (1) Fi = newF
      v) Endif
   f) Endif
   g) if Fi < $pBest_i$
      i) Update pBest & fitness_pBest
   h) Endif
   i) Assign Pbest's best individual as new_gBest
   j) If fitness_new_gBest < fgBest
      i) Update gBest & fitness_gBest
   k) Endif
5) Endfor

due to some disadvantages, it may not find the correct result (global optimum) in every problem [23]. Every day, new algorithms and new search strategies are suggested. Even if some of these methods are not good, very efficient results can be obtained when the suggested search strategies are applied to different methods. AHA (Artificial Hummingbird Algorithm) is one of the most powerful algorithms proposed so far, and the search strategies proposed for the algorithm will also shed light on the development of other algorithms. While searching for the optimal solution in the PSO algorithm and many similar algorithms, previously visited candidate solutions are repeatedly visited. Contrary to the purpose of the optimization, this causes unnecessary processing load, prolongs the optimum convergence time and prevents the discovery of different points. Instead of exploring different points, the particles go to the same points all the time, and they can get stuck in the local optimum and prevent them from reaching the global optimum. The visit table aims to ensure that the particles go to places that are not visited first and to discover at different points.

2) MATHEMATICAL MODEL OF THE ALGORITHM

This section introduces details of the proposed optimization algorithm. The pseudocode of the proposed method is given in Algorithm 1. The relevant sections are explained in detail as the following.

a: INITIALIZATION

This section introduces details of the proposed optimization algorithm. The pseudocode of the proposed method is given in Algorithm 1. The relevant sections are explained in detail as the following.

$$x = x_{low} + r.(x_{up} - x_{low}) \tag{3}$$

where x is the initial random population, r represents a random number in the range (0, 1). In the proposed method, particles are search agents and each particle is regarded as a candidate solution. The search agents are updated during the iterations. The positions' matrix of the particles and the corresponding fitness values are given as;

$$x = \begin{bmatrix} x_{11} & x_{12} & \dots & x_{1d} \\ x_{21} & x_{22} & \dots & x_{2d} \\ \vdots & \vdots & \vdots & \vdots \\ x_{n1} & x_{n2} & \dots & x_{nd} \end{bmatrix}, f(x) \begin{bmatrix} f(x_{11}, x_{12}, \dots, x_{1d}) \\ f(x_{21}, x_{22}, \dots, x_{2d}) \\ \vdots \\ f(x_{n1}, x_{n2}, \dots, x_{nd}) \end{bmatrix} \tag{4}$$

where n represents the number of the population and d is the dimension of the population. $f(x)$ represents the fitness values for *n-particles*. The visit table is initially generated as in Eq. (5):

$$VT_{ij} = \begin{cases} NaN & if i = j \\ 0 & else \end{cases} \tag{5}$$

According to Eq.(5), in the case of i=j, the particle receives food from the relevant source and the visit table is assigned as $VT_{ij} = NaN$. When the ith particle has just visited the source, then $VT_{ij} = 0$.

b: UPDATING OF PARTICLES

This section is divided into two stages as visit table strategy and multiple direction search strategy.

Visit Table Strategy

To prevent particles from constantly going to the same points and to better converge the global optimum with the discovery of different points, a visit table strategy has been added to the PSO. Accordingly, the equations of the velocity and the position in the PSO algorithm are rearranged as in Eqs. (6) and (7):

$$v_i(k+1) = v_i(k) + C_1.rand.(x_{TI}(k) - x_i(k)) + C_2.(p_{best} - x_i(k)) \tag{6}$$

$$x_i(k+1) = x_i(k) + v_i(k+1) \tag{7}$$

where, $v_i(k)$ and $v_i(k+1)$ represent the current and the next velocities, respectively. Similarly $x_i(k)$ and $x_i(k+1)$ represents the current and next positions. C is the acceleration

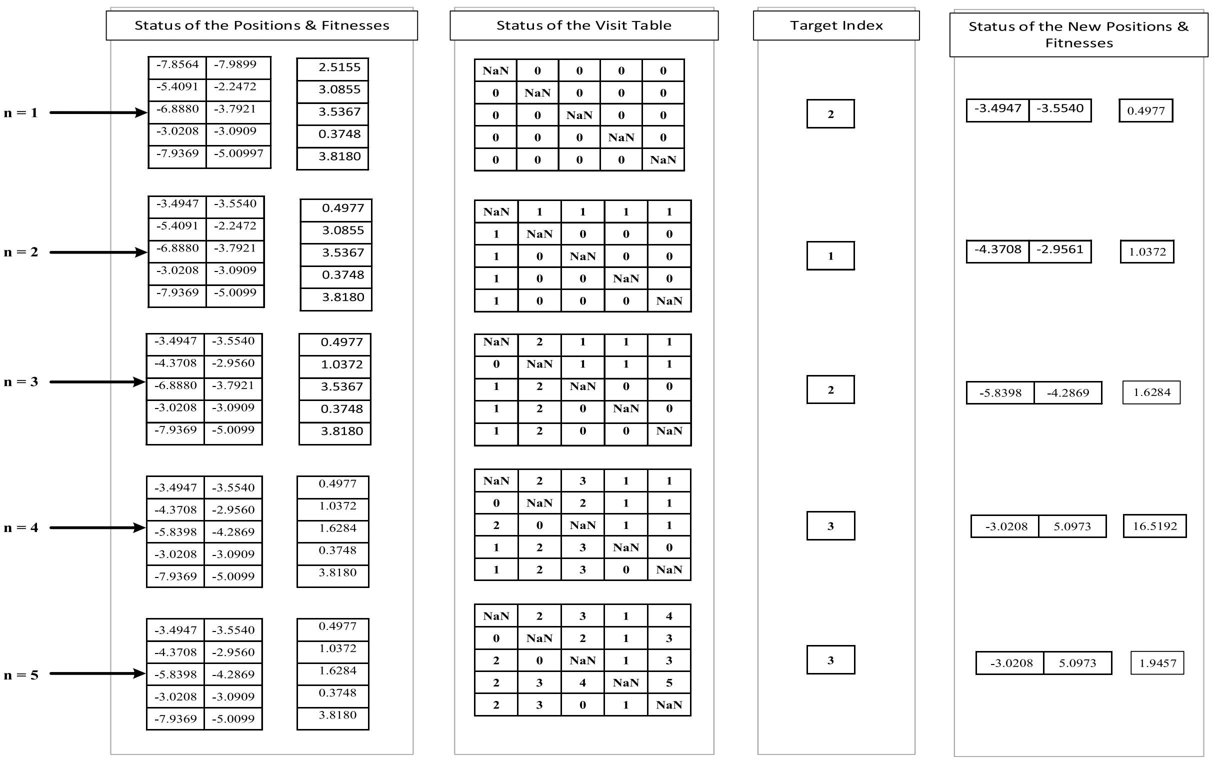

FIGURE 2. **Updating the position of particles according to the particle swarm with the visit table strategy.**

factor of the PSO. *rand* is the random number in the range of (0,1). $x_{TI}(k)$ is the individual with the highest visitation level. p_{best} represents the local best fitness value.

In the visit table, the value of each visited point is assigned as zero, and the values of the points not visited are increased by one. When guiding the swarm, the priority is to direct the swarm to places that have never been visited or least visited points. The points with the maximum value in the visit table indicate the positions of the sources that the swarm will primarily visit. Figure 2 shows how to update the position of particles according to the visit table strategy using Eqs. (6)-(7). Here, position updates and visit table changes are observed for the five particles. The visiting table is initially created according to Eq. (5). According to the created visit table, the target index is determined for the nth particle. For example, if we look for particle 1 since the target index is 2, it updates the position according to the position of particle 2 (Eqs. (6) – (7)). If the fitness value of the new solution obtained is better than the previous one, the new solution replaces the old one, otherwise, it keeps the old position. In this direction, location updates are performed for each of the five particles according to the visit levels in the visit table. In each update, the visited value in the visit table is assigned zero and the values of the unvisited points are increased by one.

Multiple Direction Search Strategy

Multiple Direction Search Strategy for PSO is constructed based on AHA [24]. To enhance the exploration ability, the positions of the particles are determined to fly in different directions from their position. Therefore, the velocity and position equations are rearranged as follows:

$$v_i\,(k+1) = v_i\,(k) + rand.DV.x_i\,(k) \tag{8}$$

$$x_i(k+1) = x_i(k) + v_i\,(k+1) \tag{9}$$

where, $v_i\,(k)$ and $v_i(k+1)$ represent the current and the next velocities, respectively. Similarly $x_i\,(k)$ and $x_i(k+1)$ represents the current and next positions. C is the acceleration factor of the PSO. *rand* is the random number in the range of (0,1).

DV denotes the direct vector and includes three versions of flight as diagonal, omnidirectional, and axial type.

$$DV\;(i) = \begin{cases} Omnidirectional, & if\left(r < \dfrac{1}{3}\right) \\ Diagonal, & if\left(\dfrac{1}{3} < r < \dfrac{2}{3}\right) \\ Axial, & if\left(r > \dfrac{2}{3}\right) \end{cases} \tag{10}$$

Direction vectors for the omnidirectional, axial, and diagonal flights are given in the following equations, respectively:

$$DV\;(i,:) = 1 \tag{11}$$

$$DV\;(i,m) = 1 \tag{12}$$

$$DV(i,1:n) = 1 \tag{13}$$

where, DV(i,:) represents the movement direction of the ith particle, $m = randperm(k)$, and $n = r_2.(D-2)+1$. The size

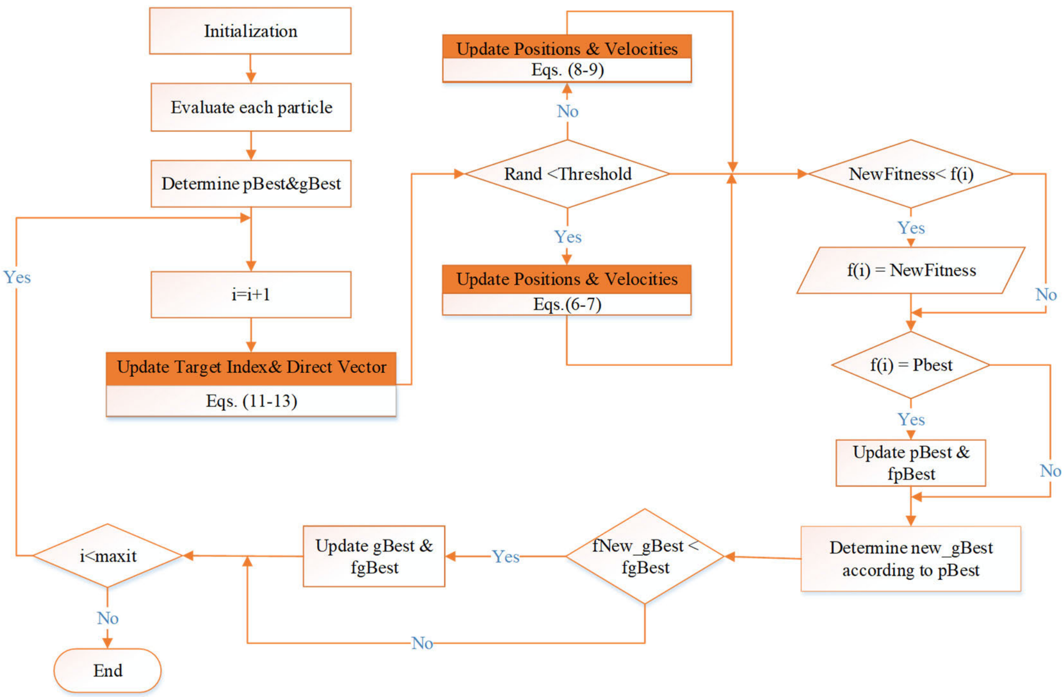

FIGURE 3. Flowchart of the improved PSO method.

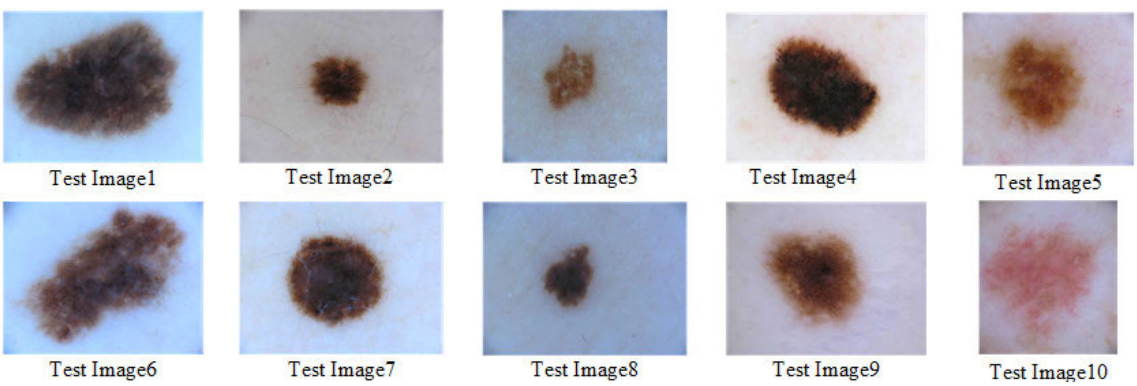

FIGURE 4. Test images of this study.

of the direct vector is determined by the dimensions of the problems.

c: CHECKING TERMINATING CONDITIONS

The optimization process will continue until the number of iterations reaches the maximum. Otherwise, it will end.

3) PROCEDURE FOR THE IMPROVED PSO

The main procedure of the proposed method is explained in this part. The pseudo-code and the flowchart of the improved PSO method are represented in Algorithm 1 and Figure 3, respectively.

Step 1: Initialization: The algorithm parameters (number of the maximum iteration as 1000, population size as 20, number of the runs as 20, Threshold value as 0.5, the acceleration factors (c_1-c_2) as 06-1.2, inertia moment as 0.8) are assigned. The initial positions and the velocities of the particles are initialized randomly in the range of search space. The fitness

TABLE 2. Hyper parameters used in the segmentation algorithm.

Definition	Parameter	Value
Inertia moment	W	0.8
Acceleration factors	C_1, C_2	0.6, 1.2
Number of the particles	Npop	20
Maximum number of iterations	Max_{iter}	1000
Number of the run	Runs	20

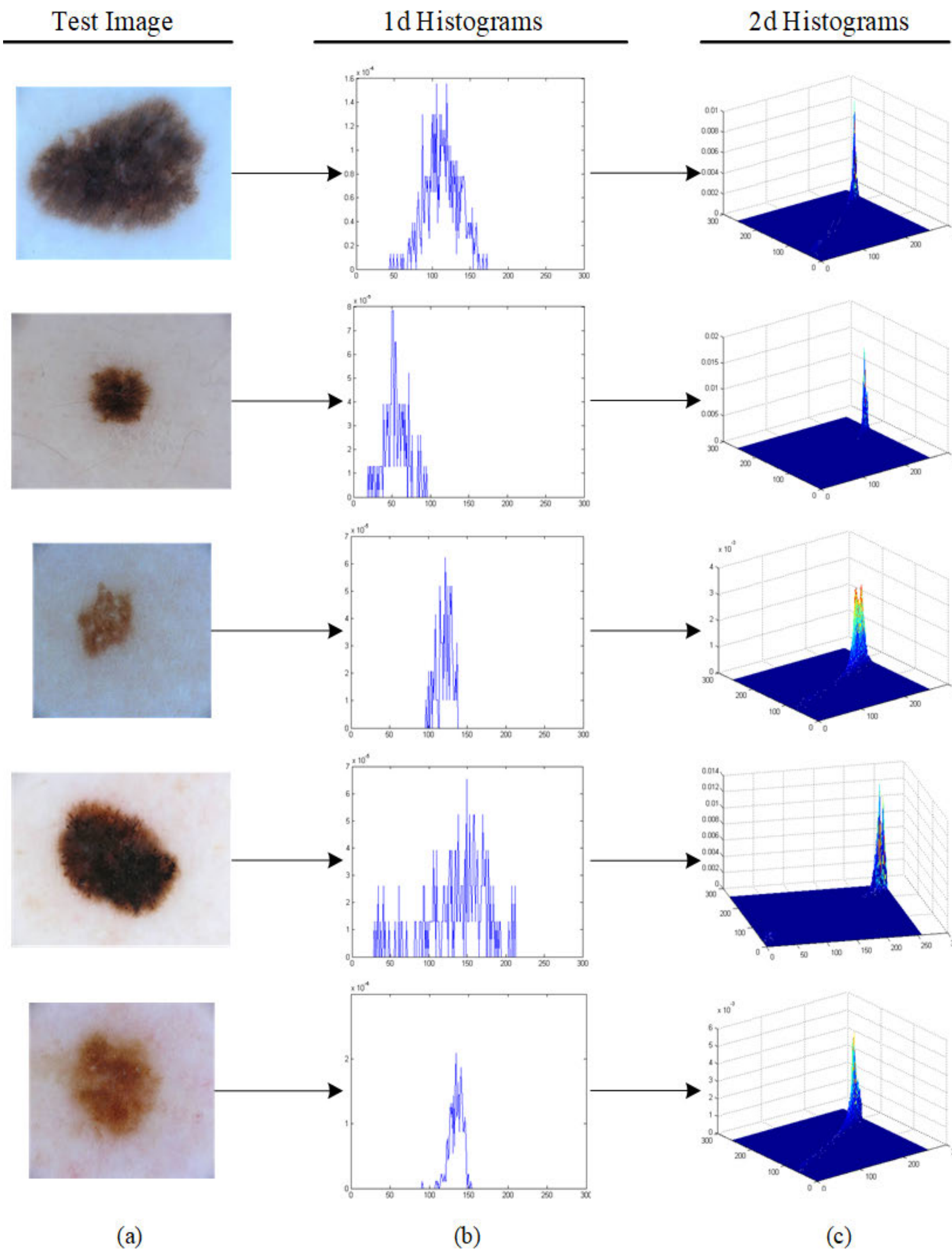

FIGURE 5. Original images and their histograms, (a)original images, (b) 1d histogram and (c) 2d histogram.

values of the particle are calculated according to objective functions. The visit table is initialized as specified in Eq. (5).

Step 2: Selection of the movement strategies: Two movement strategies are proposed for the updating of the particles. Then, according to the determined threshold value, it is determined which strategy the particles will move using.

Step 3: Update on the selected strategy: In this section, the positions and velocities of the particles are updated according to the selected strategy. The direct vector, target index, visit table, and local and global optimums are updated.

Step 4: Checking terminating conditions: If the terminating criterion is satisfied, then optimization will be terminated.

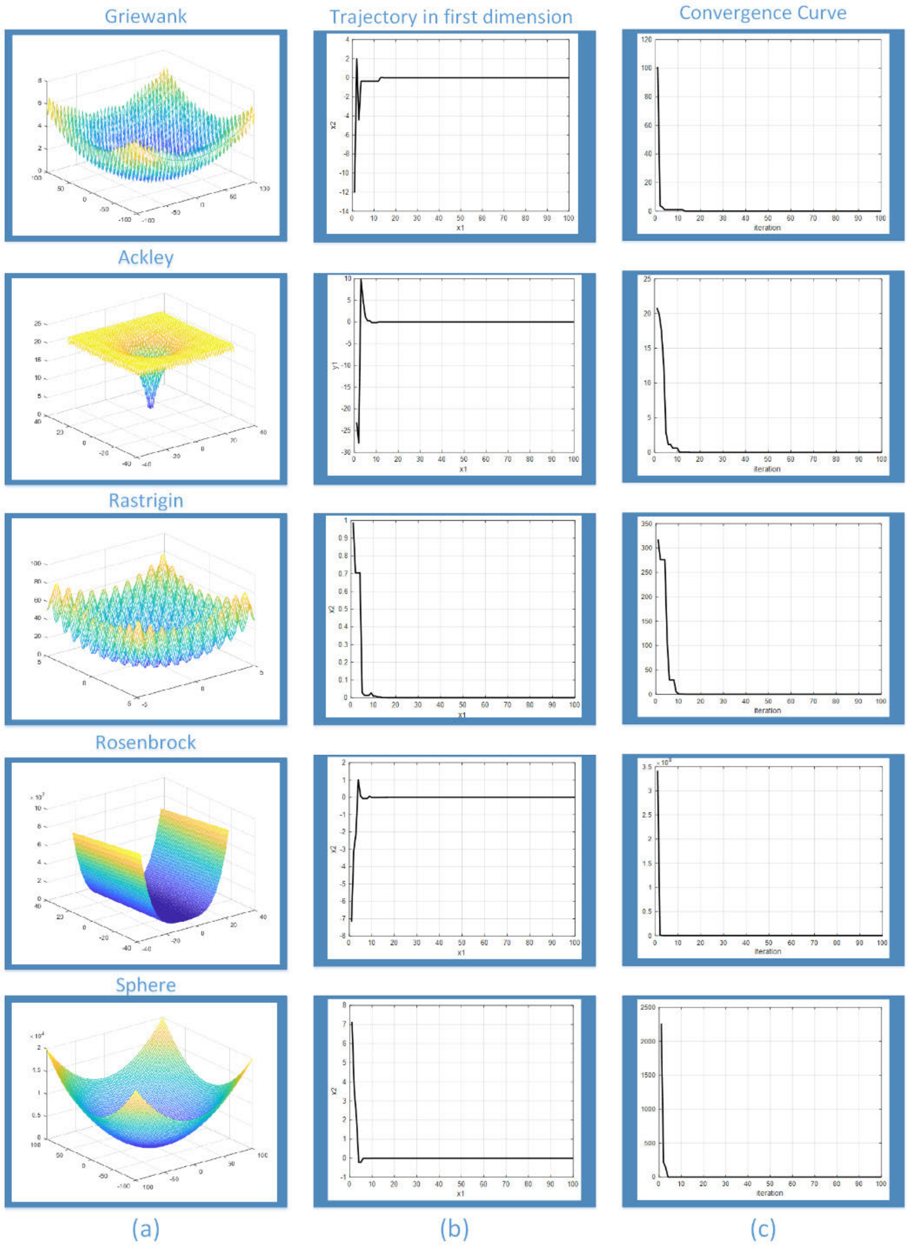

FIGURE 6. **Summary of qualitative analysis; (a) Landscape of the benchmark function, (b) Trajectory in 1st dimension, and (c) Convergence curve.**

Otherwise, it will continue from Step 2 until the number of the iteration reaches the maximum.

4) COMPUTATIONAL COMPLEXITY

Computational complexity is an important metric used to evaluate the performance of the proposed method. The proposed method has three main processes: initialization, fitness evaluation, and the updating of the particles. In the initialization, the computational complexity is *O(n)*. In the updating process, the computational complexity is *O(nT),* where *T* represents the maximum number of iterations and n is the number of particles. Thus, the computational complexity of the proposed method is O(n x (1 + T)) [25].

III. EXPERIMENTAL STUDIES

This section explains the experimental studies and results of the proposed optimization algorithm. Firstly, we used 50 benchmark functions consisting of functions with various properties, to evaluate the optimization algorithm from different perspectives. The details of the functions are given in Tables 9–10. We used ten skin cancer images from the ISIC2017 dataset for further evaluation. Selected test images are shown in Figure 4. The images are stated as

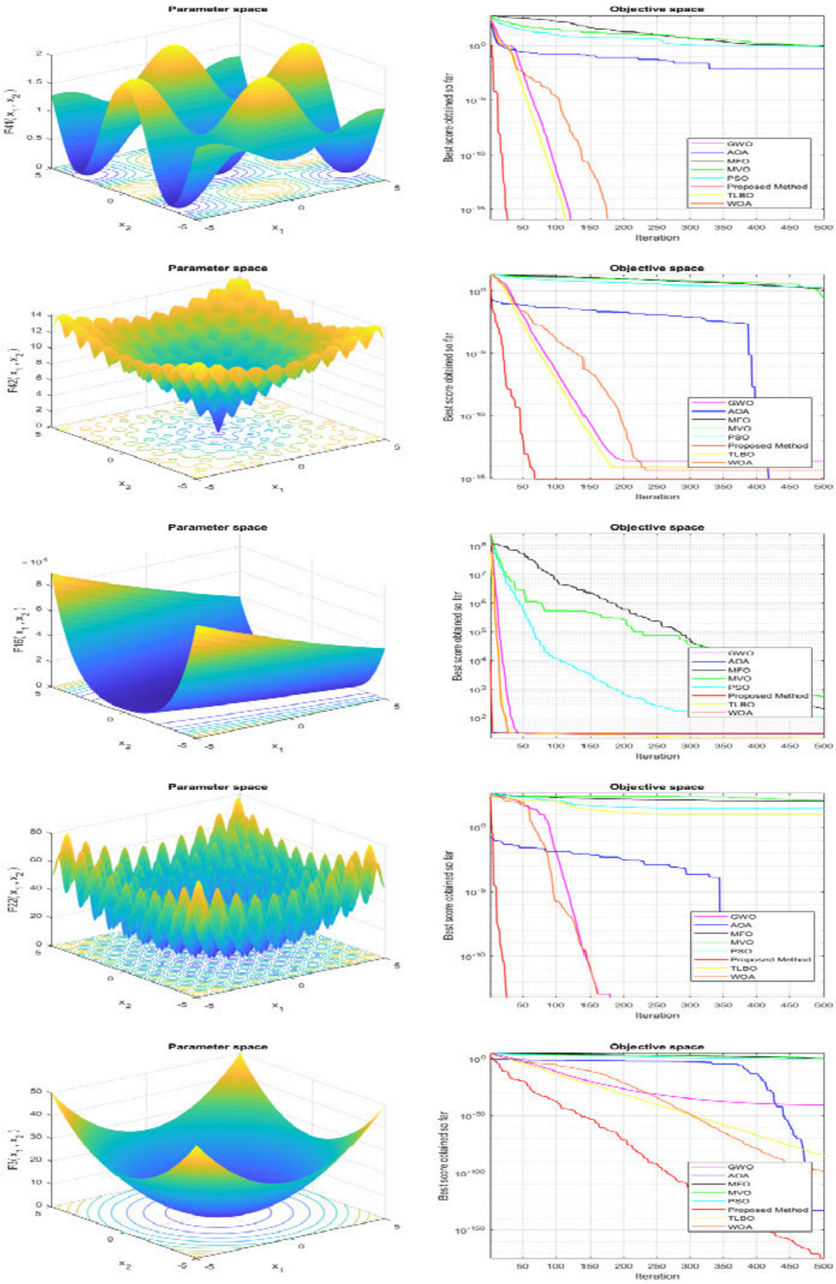

FIGURE 7. Convergence curves were obtained using functions with different algorithms.

Test Image1, Test Image2, and so on. Figure 5 displays the 1D and 2D histograms of the images. The performance of the proposed method is compared with seven state-of-the-art methods, which are AOA [26], GWO [27], MFO [28], WOA [29], MVO [30], TLBO [31], and original PSO [22].

All algorithms are tested over 20 runs with 1000 iterations for multilevel thresholding segmentation. The images are segmented with 2, 3, 4, and 5 thresholding levels. Segmented results are assessed in terms of SSIM, FSIM, and PSNR evaluation metrics. The experimental studies are performed on Matlab 2020a in a Windows 10 environment, with an Intel core-i7 (9th Gen.) processor and 16 GB RAM. This section is structured as follows: Section A presents the experimental setup, Section B represents experiments on benchmark problems, and Section C represents MTS experiments on skin cancer images.

A. EXPERIMENTAL SETUP

This section is structured as follows: Section I introduces the parameter settings, and Section II presents the evaluation metrics.

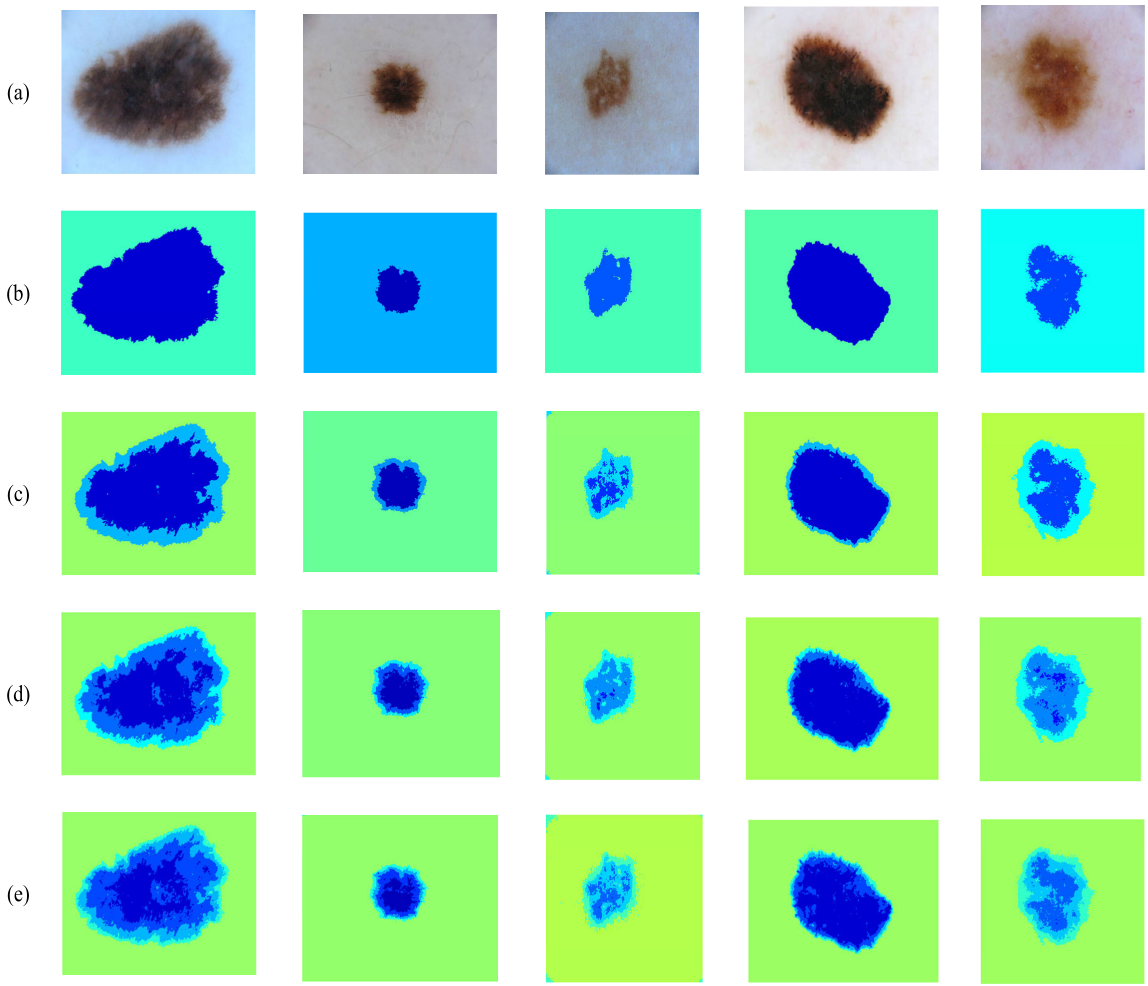

FIGURE 8. Segmented images acquired using improved PSO algorithm: (a) original images, (b) 2 level, (c) 3 level, (d) 4 level, and (e) 5 level segmented images.

1) PARAMETER SETTING

The proposed method is compared with seven algorithms: PSO, AOA, GWO, WOA, TLBO, MFO, and MVO. Algorithms are tested over 20 runs for each test image. The population size and the maximum iteration number are set as 20 and 1000 for all algorithms. The other parameter values of the proposed method are provided in Table 2. To ensure a fair comparison, basic parameters such as the number of iterations, number of runs, and population size are set the same for all considered optimization algorithms. Other parameters of the compared methods are used in their original form.

2) EVALUATION METRICS

a: PEAK SIGNAL-TO-NOISE RATIO (PSNR)

It evaluates the performance of the multilevel thresholding segmentation according to the error between the segmented image and corresponding pixels of the input image. A higher PSNR value indicates better thresholding performance. The PSNR index can be calculated as [32]:

$$PSNR = 20\log_{10}\frac{255}{\sqrt{MSE}} \tag{14}$$

$$MSE = \frac{1}{MxN}\sum_{i}^{M-1}\sum_{j}^{N-1}\left(I_{org}\left(i,j\right) - I_{seg}\left(i,j\right)\right)^2 \tag{15}$$

where MxN denotes the size of the input image. I_{org}(i,j) and I_{seg}(i,j) represent the grayscale values of the original input and segmented images, respectively.

b: FEATURE SIMILARITY INDEX (FSIM)

It is another significant index used to evaluate the thresholding segmentation performance. FSIM calculates the feature similarity between the original and segmented images based on phase consistency (PC) and gradient amplitude (G) features. A higher FSIM value indicates better segmentation performance [33].

$$FSIM\left(x,y\right) = \frac{\sum_{x\in\Omega} S_L(X)PC_m(X)}{\sum_{x\in\Omega} PC_m(x)} \tag{16}$$

$$SL\left(X\right) = S_{PC}(X)S_G(X) \tag{17}$$

$$S_{PC} = \frac{2PC_1(X) + PC_2(X) + T_1}{PC_1^2\left(X\right) + PC_2^2\left(X\right) + T_1} \tag{18}$$

TABLE 3. Renyi's optimum threshold values obtained at all levels for test images (Image 1-Image 5).

Image	nTh	IPSO	PSO	AOA	GWO	MFO	WOA	MVO	TLBO
Test Image1	2	20,110	89,152	191,236	20,110	20,105	20,110	20,110	20,110
	3	20,76,132	20,84,154	132,177,241	20,76,132	20,75,131	20,76,132	20,77,133	20,76,732
	4	14,58,95,133	118,160,199,235	88,169,207,236	20,59,97,134	20,56,94,132	20,58,96,134	20,58,95,133	20,56,91,126
	5	20,49,77,105,133	88,130,165,201,235	98,148,203,225,254	20,50,79,107,135	20,44,68,93,117	20,50,80,110,140	20,49,78,106,133	20,48,76,105,134
Test Image2	2	14,75	116,218	112,214	14,110	20,105	14,110	14,110	14,110
	3	14,68,121	98,159,218	101,151,232	14,65,121	20,75,131	14,62,121	14,68,121	14,68,121
	4	14,54,94,134	82,129,174,218	104,155,203,249	14,51,89,129	20,56,94,132	14,53,93,133	14,53,93,133	14,44,75,116
	5	14,43,73,103,133	70,113151,189,226	82,131,157,186,223	14,41,68,98,127	20,44,68,93,117	14,43,73,102,131	14,44,74,104,134	14,42,70,98,128
Test Image3	2	53,113	143,199	148,187	53,113	50,100	48,113	53,113	53,113
	3	44,88,132	53,155,210	21,77,186	42,86,132	40,79,120	40,86,132	44,88,132	41,81,121
	4	34,67,100,134	53,133,174,215	29,51,172,190	32,66,100,134	31,62,94,120	47,94,141,185	35,69,103,137	32,64,97,133
	5	28,56,84,112,140	30,67,3141,181,220	41,98,131,150,227	22,53,81,110,138	22,47,71,98,125	28,56,84,112,140	29,56,84,111,138	27,53,79,106,134
Test Image4	2	20,116	139,240	147,240	20,116	20,131	20,121	20,116	20,103
	3	20,78,135	138,189,240	120,221,248	20,78,136	20,73,125	20,78,136	20,78,136	20,78,136
	4	20,59,98,134	20,67,114,168	108,172,224,250	20,57,94,133	20,54,88,121	20,59,98,137	20,59,98,137	20,57,95,134
	5	20,48,77,106,134	55,88,126,162,197	96,148,166,212,243	20,50,78,107,136	20,51,81,112,143	20,50,78,106,134	20,46,73,100,127	20,41,63,98,132
Test Image5	2	48,97	130,204	48,86	48,97	49,105	49,68	48,97	48,97
	3	47,94,141	38,87,204	133,170,212	45,93,141	56,89,140	47,94,141	47,94,141	47,94,141
	4	35,70,106,140	49,143,185,221	151,173,213,236	30,63,97,132	31,62,93,124	33,66,98,134	35,70,105,140	33,65,98,133
	5	28,55,82,109,136	39,87,164,196,233	32,125,167,216,239	17,43,72,102,132	24,51,79,106,133	27,54,81,108,136	27,54,81,108,137	23,49,76,104,132

TABLE 4. Renyi's optimum threshold values obtained at all levels f or test images (Image 6-Image 10).

Image	nTh	IPSO	PSO	AOA	GWO	MFO	WOA	MVO	TLBO
Test Image6	2	26,113	139,217	11,219	26,113	26,113	26,113	26,113	26,113
	3	26,80,134	134,176,218	94,170,233	26,80,134	26,76,126	26,80,134	26,80,134	24,80,134
	4	26,62,98,134	26,142,190,224	139,183,194,235	25,62,98,134	25,63,102,141	26,62,98,134	26,61,97,134	26,63,101,138
	5	26,53,80,108,135	22,52,153,184,220	58,139,161,210,254	23,51,79,107,135	24,52,79,107,135	26,54,81,108,136	26,53,80,107,134	25,51,77,105,134
Test Image7	2	23,110	147,221	177,221	23,110	23,110	23,110	23,110	23,110
	3	23,78,133	127,174,221	144,196,222	23,78,133	23,76,129	23,77,133	23,78,133	23,78,133
	4	23,61,100,138	66,141,186,222	129,183,213,253	23,61,99,137	23,61,99,138	23,61,100,138	23,60,97,134	23,61,99,137
	5	23,51,79,108,136	23,414,180,210,233	19,101,152,188,236	18,43,71,100,128	21,44,67,92,117	23,51,79,107,135	23,51,79,106,134	23,51,80,110,140
Test Image8	2	24,94	125,192	132,195	24,94	24,94	24,94	24,99	24,99
	3	24,72,119	113,160,209	92,193,222	24,75,126	24,63,102	24,69,126	24,75,126	24,75,126
	4	24,58,93,127	80,125,173,215	119,203,215,239	24,58,92,127	24,53,83,113	18,52,99,127	24,58,93,127	24,58,93,127
	5	24,50,75,100,127	24,113,146,194,225	55,148,173,212,230	20,44,69,98,127	21,42,69,96,123	12,40,69,97,127	24,49,74,100,127	23,49,75,101,132
Test Image9	2	18,109	137,206	107,208	18,109	18,95	18,109	18,109	18,109
	3	18,74,130	126,168,212	94,171,224	18,72,128	18,67,116	18,74,130	18,73,128	18,74,130
	4	18,57,96,135	92,137,177,218	118,164,191,211	18,56,94,134	17,49,82,114	18,57,96,135	18,55,94,133	18,57,96,135
	5	18,47,76,105,134	17,57,113,190,224	72,136,209,220,254	18,47,74,103,131	18,47,76,104,132	18,47,76,105,134	18,45,73,101,129	18,44,71,101,132
Test Image10	2	56,111	61,121	88,191	55,111	56,111	60,120	70,140	55,111
	3	47,94,141	59,121,190	161,188,212	47,94,141	48,97,146	47,94,141	47,94,140	47,94,141
	4	35,70,105,140	54,106,150,190	63,100,203,230	33,66,102,138	35,64,96,129	35,70,105,140	35,70,106,141	34,69,104,139
	5	28,56,84,112,140	39,77,115,181,220	41,70,110,151,193	28,55,84,113,141	24,50,77,103,126	29,57,85,113,141	28,55,82,109,137	28,56,84,112,140

$$S_G = \frac{2G_1(X) + G_2(X) + T_1}{G_1^2(X) + G_2^2(X) + T_1} \tag{19}$$

where Ω indicates all pixels of the input image. T_1 and T_2 are constant values. PC_m represents the phase consistency matrix

TABLE 5. SSIM-based average values.

Test Image	nTh	IPSO	PSO	AOA	GWO	MFO	WOA	MVO	TLBO
Image 1	2	**0,5954**	0,5262	0,3544	**0,5954**	0,5873	**0,5954**	**0,5954**	**0,5954**
	3	0,6743	**0,6769**	0,4788	0,6742	0,6737	0,6742	0,6742	0,6742
	4	0,7179	0,4612	0,4444	0,7181	**0,7196**	0,7191	0,7179	0,7122
	5	0,7552	0,5120	0,4377	0,7551	0,7396	**0,7604**	0,7551	0,7586
Image 2	2	**0,7992**	0,7914	0,7824	0,6555	0,6555	**0,7992**	**0,7992**	**0,7992**
	3	0,8398	0,8135	0,8395	0,8395	**0,8469**	0,8394	0,8398	0,8398
	4	**0,8713**	0,6280	0,8316	0,8655	0,8171	0,8704	0,8704	0,8420
	5	0,8805	0,8576	0,8529	0,8725	0,7656	0,8789	**0,8829**	0,8741
Image 3	2	**0,7772**	0,6848	0,5852	**0,7772**	0,7468	0,7743	**0,7772**	**0,7772**
	3	**0,8023**	0,4710	0,6525	0,8014	0,7967	0,8002	**0,8023**	0,7979
	4	**0,8176**	0,7671	0,4467	0,8170	0,8069	0,7937	0,8169	0,8161
	5	0,8252	0,7784	0,7999	0,8254	0,8185	0,8252	**0,8270**	0,8257
Image 4	2	0,6962	0,6172	0,6284	0,6962	**0,7292**	0,7082	0,6962	0,6604
	3	**0,7668**	0,6763	0,5005	**0,7668**	0,7433	**0,7668**	0,7648	**0,7668**
	4	0,7875	**0,8299**	0,5681	0,7804	0,7516	0,7875	0,7875	0,7826
	5	0,7938	0,7520	0,6689	0,7979	**0,8130**	0,7930	0,7778	0,7973
Image 5	2	0,7247	0,6722	0,6918	0,7247	**0,7473**	0,7288	0,7247	0,7247
	3	**0,8093**	0,6847	0,6559	0,8074	0,8084	**0,8093**	**0,8093**	**0,8093**
	4	**0,8205**	0,6517	0,6275	0,8162	0,8088	0,8181	**0,8205**	0,8179
	5	**0,8372**	0,7455	0,7534	0,8227	0,8316	0,8364	0,8367	0,8284
Image 6	2	**0,6408**	0,5197	0,5124	**0,6408**	**0,6408**	**0,6408**	**0,6408**	**0,6408**
	3	**0,703**	0,5459	0,5867	**0,7030**	0,6960	**0,7030**	**0,7030**	**0,7030**
	4	0,7543	0,6487	0,5307	0,7526	**0,7564**	0,7543	0,7552	**0,7564**
	5	**0,786**	0,7323	0,7100	0,7832	0,7842	**0,7862**	0,7847	0,7846
Image 7	2	**0,6838**	0,6658	0,6708	**0,6838**	**0,6838**	**0,6838**	**0,6838**	**0,6838**
	3	**0,7662**	0,7072	0,6704	**0,7662**	0,7574	**0,7662**	**0,7662**	**0,7662**
	4	0,7917	0,7427	0,5674	0,7900	**0,7920**	0,7917	0,7845	0,7900
	5	0,8086	0,6401	0,8033	0,7909	0,7642	0,8066	0,8044	**0,8171**
Image 8	2	0,8085	**0,8398**	0,8376	0,8085	0,8085	0,8085	0,8259	0,8259
	3	**0,8899**	0,5637	0,7682	**0,8899**	0,8446	0,8885	0,8827	**0,8899**
	4	**0,9019**	0,8599	0,8351	0,9017	0,8806	0,8983	**0,9019**	**0,9019**
	5	0,9098	0,8855	0,8190	0,9085	0,9046	0,9076	**0,9102**	0,9098
Image 9	2	**0,7252**	0,6966	0,6679	**0,7252**	0,6895	**0,7252**	**0,7252**	**0,7252**
	3	0,7857	0,7244	0,7171	0,7858	0,7694	**0,7886**	**0,7886**	**0,7886**
	4	**0,8195**	0,6952	0,6667	0,8185	0,7893	**0,8195**	0,8177	**0,8195**
	5	**0,8398**	0,6459	0,7566	0,8353	0,8372	**0,8398**	0,8325	0,8369
Image 10	2	0,8266	0,7879	0,7748	**0,8269**	**0,8269**	0,7901	0,7798	0,8266
	3	**0,8247**	0,7857	0,2974	0,8223	0,8174	0,8223	0,8223	0,8223
	4	0,8429	0,8140	0,8182	0,8431	0,8355	0,8429	0,8416	**0,8437**
	5	**0,8485**	0,7969	0,8087	0,8450	0,8499	0,8458	0,8533	**0,8485**

and is calculated as $PC_m = \max(PC_1, PC_2)$, where PC_1 and PC_2 are the phase consistency of the segmented image and the input image, respectively. G represents the gradient amplitude and is calculated as:

$$G = \sqrt{G_X^2 + G_Y^2} \tag{20}$$

c: STRUCTURED SIMILARITY INDEX (SSIM)

It measures the similarity between two images. It can be calculated as [34]:

$$SSIM\ (x, y) = \frac{(2\mu_x\mu_y + c_1)(2\sigma_{xy} + c_2)}{(\mu_x^2 + \mu_y^2 + c_1)(\sigma_x^2 + \sigma_y^2 + c_2)} \tag{21}$$

where μ_x and μ_y indicate the averages of the input and segmented images. σ_x and σ_y are the standard variances of the input and segmented images. σ_{xy} refers to the covariance and the c_1, and c_2 are the constant values. A higher SSIM value refers to better segmentation performance.

B. EXPERIMENTS ON BENCHMARK PROBLEMS

The performance of the proposed method is tested with 50 benchmark functions consisting of functions with various properties to evaluate the optimization algorithm from different perspectives. The results are analyzed and compared with other optimization algorithms. The used benchmark functions are given in Tables 9–10 and more details of the functions can be found in [35]. Of the mentioned test functions, 36 are nonseparable, 14 are separable, 17 are unimodal and 33 are multimodal.

1) QUALITATIVE RESULTS

To verify the performance of the proposed method, qualitative analysis is discussed in this section. The test functions include 2 unimodal (Sphere and Rosenbrock) and 3 multimodal (Griewank, Ackley, and Rastrigin) functions. For the qualitative analysis, three subfigures, which include

TABLE 6. FSIM-based average values.

Test Image	nTh	IPSO	PSO	AOA	GWO	MFO	WOA	MVO	TLBO
Image 1	2	0,6886	**0,6947**	0,6803	0,6886	0,6861	0,6886	0,6886	0,6886
	3	0,7029	0,6978	0,6983	**0,7031**	**0,7031**	**0,7031**	0,7028	**0,7031**
	4	0,6939	0,7068	0,7305	0,7300	**0,7342**	0,7311	0,7305	0,7309
	5	**0,7623**	0,7236	0,6980	0,7583	0,7505	0,7583	0,7579	0,7612
Image 2	2	**0,7023**	**0,7023**	0,7021	0,7022	0,6961	0,7022	0,6961	0,7022
	3	0,7056	**0,7102**	0,7063	0,7047	0,7052	0,7043	0,7052	0,7052
	4	**0,7384**	0,7113	0,7073	0,7081	0,7078	0,7071	0,7071	0,7091
	5	0,7131	**0,7530**	0,7475	0,7141	0,7067	0,7127	0,7130	0,7134
Image 3	2	**0,6208**	0,6197	0,6207	**0,6208**	0,6187	0,6203	**0,6208**	**0,6208**
	3	0,6256	0,5455	0,6133	0,6294	**0,6299**	0,6289	0,6298	0,6263
	4	0,6620	**0,6689**	0,6349	0,6346	0,6287	0,6309	0,6355	0,6343
	5	0,6415	0,6387	0,7426	0,6409	0,6347	0,6415	0,6419	0,6387
Image 4	2	**0,7302**	0,7284	0,7279	**0,7302**	0,7299	**0,7302**	**0,7302**	**0,7302**
	3	**0,7434**	0,7335	0,7149	**0,7434**	**0,7434**	**0,7434**	**0,7434**	**0,7434**
	4	0,7382	0,7544	0,7574	0,7577	0,7569	0,7574	0,7574	**0,7579**
	5	0,7694	**0,7718**	0,7476	0,7700	0,7714	0,7699	0,7686	0,7706
Image 5	2	0,7037	0,7046	0,7016	0,7037	**0,7056**	0,7045	0,7037	0,7037
	3	**0,7138**	0,6990	0,7102	0,7131	0,7133	0,7133	0,7133	0,7133
	4	0,7116	0,7119	0,7165	0,7158	0,7152	**0,7166**	**0,7166**	0,7163
	5	**0,7231**	0,7452	0,7094	0,7190	0,7213	**0,7231**	0,7228	0,7207
Image 6	2	**0,7104**	0,7047	0,7072	**0,7104**	**0,7104**	**0,7104**	**0,7104**	**0,7104**
	3	**0,7244**	0,7075	0,7152	**0,7244**	0,7229	**0,7244**	**0,7244**	**0,7244**
	4	**0,7455**	0,7027	0,7085	0,7444	0,7453	0,7450	0,7447	**0,7455**
	5	**0,7610**	0,7256	0,7414	0,7589	0,7597	0,7603	0,7598	0,7593
Image 7	2	**0,6975**	0,6949	0,6865	**0,6975**	**0,6975**	**0,6975**	**0,6975**	**0,6975**
	3	**0,7112**	0,7032	0,6869	**0,7112**	0,7106	**0,7111**	**0,7112**	**0,7112**
	4	0,7084	0,7029	0,7216	0,7217	**0,7218**	0,7216	0,7214	0,7217
	5	0,7338	0,6940	0,7119	0,7315	0,7289	0,7334	0,7332	**0,7350**
Image 8	2	0,7178	0,7137	**0,7204**	0,7172	0,7172	0,7172	0,7172	0,7178
	3	0,7186	0,6762	0,7155	**0,7203**	0,7159	0,7198	**0,7203**	**0,7203**
	4	0,7129	**0,7275**	0,7255	0,7255	0,7226	0,7246	0,7255	0,7255
	5	**0,7294**	0,7283	0,7288	0,7288	0,7239	0,7283	**0,7294**	0,7293
Image 9	2	**0,7123**	0,7105	0,7108	**0,7123**	0,7119	**0,7123**	**0,7123**	**0,7123**
	3	0,7154	0,7115	**0,7193**	0,7144	0,7153	0,7153	0,7147	0,7153
	4	**0,7449**	0,7361	0,7215	0,7214	0,7205	0,7215	0,7212	0,7215
	5	**0,7285**	0,7240	0,7139	0,7281	0,7281	0,7285	0,7278	0,7279
Image 10	2	0,7354	0,7121	**0,7598**	0,7268	0,7269	0,7125	0,7269	0,7268
	3	**0,7536**	0,7115	0,7386	0,7463	0,7463	0,7463	0,7435	0,7463
	4	**0,8102**	0,7674	0,7536	0,7451	0,7302	0,7536	0,7574	0,7485
	5	0,7723	0,7669	**0,7735**	0,7720	0,7338	0,7663	0,7532	0,7663

(a) functions' landscape, (b) trajectory in the 1st dimension, and (c) convergence curve of the global best particle for each function are given in Figure 5.

Figure 6 represents the convergence curves of 2 unimodal (Sphere-F3 and Rosenbrock-F16) and 3 multimodal (Griewank-F41, Ackley-F42, and Rastrigin-F22) functions for all algorithms (AOA, WOA, GWO, MVO, MFO, TLBO, PSO and the improved PSO), comparatively.

The dimension and the number of the iterations are set as 30 and 1000, respectively. As seen in Figure 7, the improved PSO algorithm achieved the fastest convergence for these unimodal and multimodal functions.

2) QUANTITATIVE ANALYSIS

The statistical analysis is presented in Tables 12-15. The results are provided with 20 independent runs for each test function. According to the average values obtained after 20 runs, the proposed method succeeded in 60% of the applied test functions. However, PSO 18%, AOA 20%, GWO 30%, MFO 26%, WOA 24%, MVO 18%, and TLBO 48% were more successful than the other methods. According to the minimum values obtained after 20 runs, the proposed method was successful in 62% and PSO 18%, OA 20%, GWO 30%, MFO 26%, WOA 24%, MVO 18% and TLBO 48% of the 50 benchmark functions. According to the maximum values, the improved PSO method was successful in 42% of the applied test functions. However, PSO 20%, AOA 26%, GWO 26%, MFO 26%, WOA 16%, MVO 18%, and TLBO 56% were more successful than other methods. According to the standard deviation values, the proposed method was successful in 46% and PSO 18%, AOA 20%, GWO 14%, MFO 18%, WOA 12%, MVO 4% and TLBO 48% of the 50 benchmark functions.

TABLE 7. PSNR-based average values.

Test Image	nTh	IPSO	PSO	AOA	GWO	MFO	WOA	MVO	TLBO
Image 1	2	**14,0204**	10,7312	10,1710	10,7312	10,3919	10,7312	10,7312	10,7312
	3	**15,4191**	13,2447	13,9163	13,2447	13,1516	13,2447	13,3381	13,2447
	4	15,0235	13,6785	**15,9447**	13,7822	13,5794	13,7907	13,6785	12,9248
	5	**15,3961**	17,0728	13,8291	14,0632	12,0926	14,6875	13,8271	13,9528
Image 2	2	**13,1088**	8,7163	12,5948	12,4469	8,7163	12,4469	12,4469	12,4469
	3	**20,6931**	14,1940	19,7124	14,1957	14,8580	14,1967	14,1940	14,1940
	4	18,3574	16,6771	**20,4183**	15,6782	12,2015	16,4712	16,4712	13,4717
	5	**22,0453**	20,5861	16,3204	15,3399	10,4179	16,1155	16,7431	15,5273
Image 3	2	**15,2375**	15,0386	13,7220	15,0386	13,0353	14,9759	15,0386	15,0386
	3	13,9926	**19,2385**	10,2507	19,2389	16,5466	19,2139	19,2384	16,7512
	4	18,7880	20,0247	8,0390	20,0115	16,5884	**21,3932**	20,9133	19,7180
	5	**23,8915**	20,4459	22,0435	21,3776	17,7390	22,0435	21,3925	20,1416
Image 4	2	10,4051	8,8176	**11,0498**	8,8176	10,0307	9,2095	8,8176	7,8615
	3	**15,6960**	10,5661	13,1799	10,6619	9,6582	10,6619	10,6619	10,6619
	4	**14,5063**	10,8206	16,6157	10,4321	9,3507	10,8206	10,8206	10,5285
	5	**19,2812**	19,1116	10,5528	10,7471	11,4699	10,5499	9,8970	10,3695
Image 5	2	**12,4688**	10,6291	9,5888	10,6291	11,4505	10,7330	10,6291	10,6291
	3	9,6490	**16,5229**	15,0733	16,4904	16,3352	16,5229	16,5229	16,5229
	4	**17,4187**	16,5955	13,5351	15,2231	14,0129	15,5591	16,5962	15,3934
	5	18,2747	**18,6564**	15,9758	15,2558	15,4428	15,9710	16,1473	15,2733
Image 6	2	**11,2975**	10,8821	10,0799	10,8821	10,8821	10,8821	10,8821	10,8821
	3	13,5471	13,4035	**14,9966**	13,4035	12,6151	13,4035	13,4035	13,4035
	4	**15,8567**	13,7892	13,6969	13,7829	14,6616	13,7892	13,7933	14,2841
	5	16,4859	**17,9054**	14,0293	14,0223	14,0273	14,1594	13,9016	13,9035
Image 7	2	**12,0777**	9,2195	13,9620	9,2195	9,2195	9,2195	9,2195	9,2195
	3	**15,4404**	11,5266	16,7819	11,5266	11,1048	11,5282	11,5266	11,5266
	4	**18,5956**	12,2068	16,9321	12,0886	12,2071	12,2068	11,7458	12,0886
	5	**19,4828**	19,1316	12,0277	11,1292	10,0258	11,9103	11,7943	12,5118
Image 8	2	16,5345	12,2607	**17,2722**	12,2607	12,2607	12,2607	12,9369	12,9369
	3	17,4534	16,4543	11,8762	17,9911	13,4576	17,9860	**17,9911**	**17,9911**
	4	17,3710	18,4014	15,6717	18,4001	15,3465	18,3824	**18,4014**	**18,4014**
	5	19,3693	**22,9668**	18,4769	18,4724	17,4796	18,4655	18,4779	18,4752
Image 9	2	**13,0235**	11,1657	10,7426	11,1657	9,8760	11,1657	11,1657	11,1657
	3	16,8327	13,9854	**17,7054**	13,7233	12,2324	13,9854	13,7206	13,9854
	4	**19,0988**	14,9549	17,5957	14,8010	12,0856	14,9549	14,6498	14,9549
	5	14,5579	14,0562	**14,8996**	14,4277	14,5823	14,8996	14,1255	14,5814
Image 10	2	**16,1799**	14,9669	11,6502	14,9644	14,9669	16,0845	14,9644	14,9644
	3	16,1297	**19,4953**	7,4963	19,4953	19,9517	19,4953	19,4953	19,4953
	4	**21,1894**	20,5022	13,2727	19,9723	18,1939	20,5023	20,2770	20,2770
	5	**21,7917**	15,8427	20,9791	21,2171	17,8390	21,2253	20,9793	20,9793

3) SCALABILITY ANALYSIS

This section evaluates the proposed algorithm against other algorithms with problems of different sizes. The experimental results on 3 dimensions 10, 50, and 100 in terms of mean and standard deviation are given in Tables 16-18 for 25 benchmark functions, respectively. Regarding the 10 dimensions, the proposed method ranked first in 10 of the 25 functions and second in 5 of the 25 functions, while in the standard deviation values, it ranked first in 10 and second in 7 of the functions. In 50 dimensions, the proposed method ranked first in 12 of the 25 functions and second in 5 of the 25 functions, while in the standard deviation values, it ranked first in 12 and second in 11 of the functions. Finally, regarding the 100 dimensions, improved PSO achieved the best average and best standard deviation in 14 and 7 test functions, respectively.

C. EXPERIMENTS ON SKIN CANCER IMAGES

To further illustrate the effectiveness of the proposed optimization algorithm, multilevel thresholding was performed using 10 skin cancer images obtained from the ISIC2017 dataset. We used Renyi's entropy as the objective function, detailed in Section II-A. Segmented images obtained by the proposed method are illustrated in Figure 8 with varying thresholding levels [n = 2, 3, 4, and 5]. The experimental results were compared with the state-of-the-art methods: PSO, AOA, GWO, MFO, WOA, MVO, and TLBO. The best thresholds acquired by the proposed

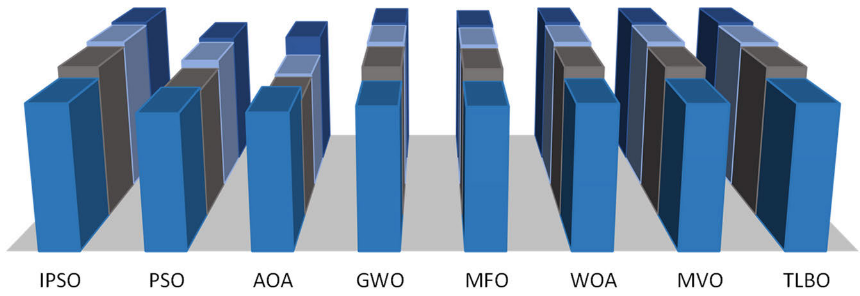

	IPSO	PSO	AOA	GWO	MFO	WOA	MVO	TLBO
level 2	0,7278	0,6802	0,6835	0,7134	0,7116	0,7254	0,7248	0,7259
level 3	0,7862	0,6649	0,6167	0,7856	0,7754	0,7858	0,7853	0,7858
level 4	0,8125	0,7098	0,6336	0,8103	0,7958	0,8096	0,8114	0,8082
level 5	0,8285	0,7346	0,741	0,8237	0,8108	0,828	0,8264	0,8281

FIGURE 9. **Average SSIM obtained for all skin cancer images.**

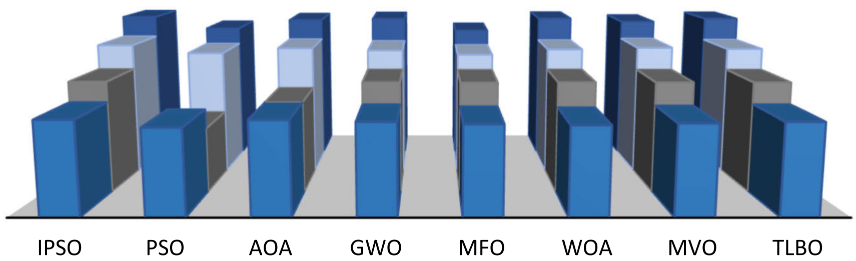

	IPSO	PSO	AOA	GWO	MFO	WOA	MVO	TLBO
level 2	0.7019	0.6986	0.7018	0.7010	0.7000	0.6996	0.7004	0.7010
level 3	0.7112	0.6896	0.7018	0.7110	0.7108	0.7110	0.7109	0.7109
level 4	0.7229	0.7190	0.7214	0.7204	0.7183	0.7209	0.7217	0.7211
level 5	0.7332	0.7271	0.7315	0.7322	0.7259	0.7324	0.7307	0.7323

FIGURE 10. **Average FSIM obtained for all skin cancer images.**

method and other metaheuristic methods are presented in Tables 3 and 4.

The average values of SSIM, FSIM, and PSNR evaluation metrics are represented in Tables 5, 6, and 7, respectively. Higher SSIM, FSIM, and PSNR average values indicate more accurate and efficient multilevel thresholding segmentation methods. The average values of SSIM for 20 runs are given in Table 5; a higher SSIM value represents a better segmentation result. The improved PSO algorithm outperforms the original PSO and AOA for nearly all threshold levels and images. GWO has competitive results with the improved PSO method at only threshold level 2 for some images. MFO gives better results at Test Images 6 and 7 for thresholds levels 2 and 4 according to the proposed method. Improved PSO has higher SSIM values at nearly all threshold levels in the remaining images. WOA performed well on Test Image 9, while the proposed method outperformed most of the remaining test images. MVO and TLBO methods have competitive results with the proposed method at threshold levels 2 and 3.

Table 6 presents the average FSIM values for each skin cancer image. The more efficient algorithm must have a higher FSIM value. When the proposed method is compared with

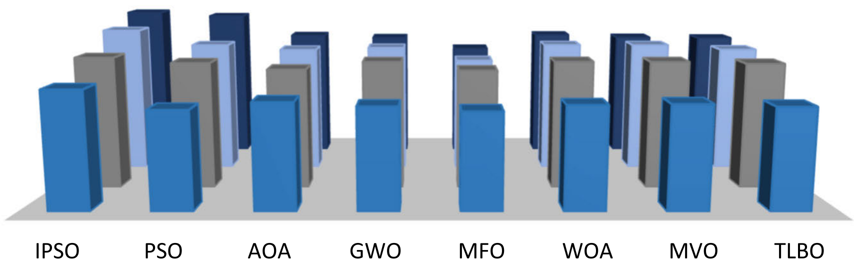

	IPSO	PSO	AOA	GWO	MFO	WOA	MVO	TLBO
level 2	13.4354	11.2428	12.0853	11.6156	11.0830	11.7709	11.8762	11.5876
level 3	15.4853	14.8631	14.0989	14.9971	13.9911	15.0239	15.0040	14.7777
level 4	17.6205	15.7651	15.1722	15.4172	13.8228	15.7870	15.7799	15.2042
level 5	19.0576	18.5776	15.9134	15.6052	14.1116	16.0028	15.6539	15.5716

FIGURE 11. Average PSNR obtained for all skin cancer images.

the original PSO and AOA methods, the proposed method has higher average FSIM values for nearly all images and threshold levels. PSO has better results at threshold level 2 for Test Images 1 and 2. GWO outperforms at threshold levels 3 for Test Images 1, 4, 6, and 7. MFO and MVO algorithms also performed well at threshold levels 2 and 3 for some test images. TLBO has competitive results with the improved PSO method test images 3, 5, and 6. Table 6 represents the average PSNR values for each image. It is seen that the proposed method outperformed the other algorithms for nearly all threshold levels at all images. Original PSO performed well at threshold level 3 for Images 3, 5, and 10. AOA performed well at threshold level 4 for Images 1 and 2. The other algorithms have lower PSNR values than the proposed method at all images and threshold levels, indicating a lower segmentation performance.

The average SSIM values for all skin cancer images are illustrated in Figure 9. The values are obtained by averaging the SSIM index of 10 skin cancer images over 20 runs. It can be noted from this figure that the improved PSO method has higher SSIM values, which indicates better multilevel segmentation performance. It is also seen that the value of the SSIM evaluation metric increases, and the level of the threshold increases. The proposed method achieves better segmentation at threshold 2 with 0.7278, threshold 3 with 0.7862, threshold 4 with 0.8125, and threshold 5 with 0.8285.

The average values of FSIM are represented in Figure 10. The values are obtained by averaging FSIM values of all skin cancer images over 20 independent runs. The FSIM values acquired by the proposed method are higher than the FSIM values acquired by other compared algorithms at threshold 2 with 0.7019, at threshold 3 with 0.7112, at threshold 4 with 0.7229, and threshold 5 with 0.7332. The AOA and TLBO also have higher FSIM values according to the remaining algorithms.

TABLE 8. Significant results of the proposed method.

No	Significant Results
1	In the qualitative analysis, the proposed method achieved faster convergence than the other metaheuristics.
2	The quantitative analysis produced more successful results compared to other methods in 60% of the applied 50 benchmark functions according to the average values.
3	In the scalability analysis, the proposed method ranked first in 10 of the 25 functions and second in 5 of the 25 functions in terms of minimum values for 10 dimensions, while it ranked first in 10 of the functions and second in 7 in terms of standard deviation values
4	The proposed optimization algorithm outperformed other algorithms for almost all threshold levels and images.
5	In the applications of skin cancer image segmentation, the best results were obtained with 0.8285 in SSIM index, 0.7332 in FSIM index, and 19.0576 in PSNR index using the proposed method according to the average values of evaluation metrics for all images.

Figure 11 represents the average PSNR values for all skin cancer images. The values are acquired by averaging PSNR values for all images over 20 independent runs. The best of average PSNR values are obtained by the proposed method at threshold level 2 with 13.4354, at threshold 3 with 15.4853,

TABLE 9. Benchmark functions (F_1-F_{24}).

No	Function Name	Formula	F_{opt}	Type	Range	D
F_1	Stepint	$f(x) = 25 + \sum_{i=1}^{n} x_i$	0	Unimodal-Separable	[-5.12,5.12]	5
F_2	Step	$f(x) = \sum_{i=1}^{n} (\lvert x_i + 0.5 \rvert)^2$	0	Unimodal-Separable	[-100,100]	30
F_3	Sphere	$f(x) = \sum_{i=1}^{n} (x_i)^2$	0	Unimodal-Separable	[-100,100]	30
F_4	Sumsquares	$f(x) = \sum_{i=1}^{n} (ix_i)^2$	0	Unimodal-Separable	[-10,10]	30
F_5	Quartic	$f(x) = \sum_{i=1}^{D} ix_i^4$	0	Unimodal, Separable	[-1.28,1.28]	D
F_6	Beale	$f(x) = (1.5 - x_1 + x_1x_2)^2 + (2.25 - x_1 + x_1{x_2}^2)^2$	0	Unimodal, Nonseparable	[-4.5,4.5]	5
F_7	Easom	$f(x) = -\cos(x_1)\cos(x_2)e^{-(x_1-\pi)^2-(x_2-\pi)^2}$	-1	Unimodal, Nonseparable	[-100,100]	2
F_8	Matyas	$f(x) = 0.26({x_1}^2 + {x_2}^2) - 0.48{x_1}^2{x_2}^2$	0	Unimodal, Nonseparable	[-10,10]	2
F_9	Colville	$f(x) = 100(x_1 - x_2)^2 + (x_1 - 1)^2 + (x_4 - 1)^2 + 90({x_3}^2 - x_4)^2 + 10.1((x_2 - 1)^2 + ((x_4 - 1)^2))$	0	Unimodal, Nonseparable	[-10,10]	4
F_{10}	Trid6	$f(x) = \sum_{i=1}^{n} (x_i - 1)^2 + \sum_{i=2}^{n} x_i x_{i-1}$	-50	Unimodal, Nonseparable	[-D^2,D^2]	6
F_{11}	Trid10	$f(x) = \sum_{i=1}^{n} (x_i - 1)^2 + \sum_{i=2}^{n} x_i x_{i-1}$	-210	Unimodal, Nonseparable	[-D^2,D^2]	10
F_{12}	Zakharov	$f(x) = \sum_{i1}^{n} x_i^2 + (\frac{1}{2}\sum_{i1}^{n} ix_i)^2 + (\frac{1}{2}\sum_{i1}^{n} ix_i)^4$	0	Unimodal, Nonseparable	[-5,10]	D10
F_{13}	Powell	$f(x) = \sum_{i=1}^{n/k} (x_{4i-3} + 10x_{4i-2})^2 + 5(x_{4i-1} + 10x_4)^2 + 5(x_{4i-2} + 10x_{4i-1})^4 + (x_{4i-1} + 10x_4)^4$	0	Unimodal, Nonseparable	[-4,5]	24
F_{14}	Schwefel 2.22	$f(x) = \sum_{i=1}^{n} \lvert x_i \rvert + \prod_{i=1}^{n} \lvert x_i \rvert$	0	Unimodal, Nonseparable	[-10,10]	30
F_{15}	Schwefel 1.2	$f(x) = \sum_{i=1}^{n} (\sum_{j=1}^{n} x_j)^2$	0	Unimodal, Nonseparable	[-100,100]	30
F_{16}	Rosenbrock	$f(x) = \sum_{i=1}^{D-1} (100(x_{i+1} - x_i^2)^2 + (x_i - 1)^2)$	0	Unimodal, Nonseparable	[-30,30]	30
F_{17}	Dixon–Price	$f(x) = (x_1 - 1)^2 + \sum_{i=2}^{n} i({x_i}^2 - x_{i-1})^2$	0	Unimodal, Nonseparable	[-10,10]	30
F_{18}	Foxholes	$f(x) = \left[\frac{1}{500} + \sum_{J=1}^{25} \frac{1}{j + \sum_{J=1}^{2} (x_i - a_{ij})^6}\right]^{-1}$	0	Multimodal, Separable	[-65.536, 65.536]	2
F_{19}	Branin	$f(x) = x_2 - \frac{5.1}{4\pi^2}{x_1}^2 + \frac{5.1}{\pi}x_1 - 6)^2 + 10\left(1 - \frac{1}{8\pi}\right)\cos x_1 + 10$	0.998	Multimodal, Separable	[-5,10] x [0,15]	2
F_{20}	Bohachevsky1	$f(x) = x_1^2 + 2x_2^2 - 0.3\cos(3\pi x_1) - 0.4\cos(4\pi x_2) + 0.7$	0.398	Multimodal, Separable	[-100,100]	2
F_{21}	Booth	$f(x) = x_1^2 + 2x_2^2 - 7)^2 + (2x_1 + x_2 - 5)^2$	0	Multimodal, Separable	[-10,10]	2
F_{22}	Rastrigin	$f(x) = -\sum_{i=1}^{n} [x_i^2 - 10\cos(2\pi x_i) + 10]$	0	Multimodal, Separable	[-5.12,5.12]	30
F_{23}	Schwefel	$f(x) = -\sum_{i=1}^{n} x_i \sin(\sqrt{\lvert x \rvert})$	0	Multimodal, Separable	[-500,500]	30
F_{24}	Michalewicz2	$f(x) = -\sum_{i=1}^{n} \sin(x_i)(\sin\left(\frac{i{x_i}^2}{\pi}\right))^{20}$	-12569	Multimodal, Separable	[0,π]	2

TABLE 10. Benchmark functions (F_{25}-F_{44}).

No	Function Name	Formula	F_{opt}	Type	Range	D
F_{25}	Michalewicz5	$f(x) = -\sum_{i=1}^{n} \sin(x_i)(\sin\left(\frac{i{x_i}^2}{\pi}\right))^{20}$	-1.8013	Multimodal, Separable	[0,π]	5
F_{26}	Michalewicz10	$f(x) = -\sum_{i=1}^{n} \sin(x_i)(\sin\left(\frac{i{x_i}^2}{\pi}\right))^{20}$	-4.6877	Multimodal, Separable	[0,π]	10
F_{27}	Schaffer	$f(x) = 0.5 + \frac{sin^2\left(\sqrt{x_1^2+x_2^2}\right) - 0.5}{(1+0.001(x_1^2+x_2^2))^2}$	-9.6602	Multimodal, Non-Separable	[-100,100]	2
F_{28}	Six Hump Camel Back	$f(x) = 4x_1^2 - 2.1x_1^4 + \frac{1}{3}x_1^6 + x_1x_2 - 4x_2^2 + 4x_2^4$	0	Multimodal, Non-Separable	[-5,5]	2
F_{29}	Bohachevsky2	$f(x) = x_1^2 - 2x_2^2 + 0.3\cos(3\pi x_1)\,(4\pi x_3) + 0.3$	-1.0316	Multimodal, Non-Separable	[-100,100]	2
F_{30}	Bohachevsky3	$f(x) = x_1^2 - 2x_2^2 + 0.3\cos(3\pi x_1)\,(4\pi x_3) + 0.3$	0	Multimodal, Non-Separable	[-100,100]	2
F_{31}	Shubert	$f(x) = \left(\sum_{i=1}^{5} icos(i+1)x_1 + i\right) + \left(\sum_{i=1}^{5} icos(i+1)x_2 + i\right)$	-186.730	Multimodal, Non-Separable	[-10,10]	2
F_{32}	GoldStein–Price	$f(x) = [1 + (x_1 + x_2 + 1)^2(19 - 14x_1 + 3x_1^2 - 14x_2 + 6x_1x_2 + 3x_2^2)]$	3	Multimodal, Non-Separable	[-2,2]	2
F_{33}	Kowalik	$f(x) = \sum_{i=1}^{11} \left\lvert a_i - \frac{x_1(b_i^2 + b_ix_2)}{b_i^2 + b_ix_3 + x_4}\right\rvert^2$	0.00031	Multimodal, Non-Separable	[-5,5]	4
F_{34}	Shekel5	$f(x) = -\sum_{i=1}^{5} \lvert(x_i - a_i)(x_i - a_i)^T + c_i\rvert^{-1}$	-10.1532	Multimodal, Non-Separable	[0,10]	4
F_{35}	Shekel7	$f(x) = -\sum_{i=1}^{7} \lvert(x_i - a_i)(x_i - a_i)^T + c_i\rvert^{-1}$	-10.4028	Multimodal, Non-Separable	[0,10]	4
F_{36}	Shekel10	$f(x) = -\sum_{i=1}^{10} \lvert(x_i - a_i)(x_i - a_i)^T + c_i\rvert^{-1}$	-10.5363	Multimodal, Non-Separable	[0,10]	4
F_{37}	Perm	$f(x) = \sum_{k=1}^{n}(\sum_{i=1}^{n}(i^k + \beta)({}^{x_i}/_{i})^k - 1))^2$	0	Multimodal, Non-Separable	[-D,D]	4
F_{38}	PowerSum	$f(x) = \sum_{k=1}^{n}(\left(\sum_{i=1}^{n} x_i^k\right) - b_k)^2$	0	Multimodal, Non-Separable	[0,D]	4
F_{39}	Hartman3	$f(x) = -\sum_{i=1}^{4} \exp[-\sum_{j=1}^{3} a_{ij}(x_j - p_{ij})^2]$	-3.86	Multimodal, Non-Separable	[0,1]	3
F_{40}	Hartman6	$f(x) = -\sum_{i=1}^{4} \exp[-\sum_{j=1}^{6} a_{ij}(x_j - p_{ij})^2]$	-3.32	Multimodal, Non-Separable	[0,1]	6
F_{41}	Griewank	$f(X) = \frac{1}{4000}\sum_{i=1}^{D} x_i^2 - \prod_{i=1}^{D}\cos\left(\frac{x_i}{\sqrt{i}}\right) + 1$	0	Multimodal, Non-seperable	[-600, 600]	D
F_{42}	Ackley	$f(x) = -20\exp(-0.2\sqrt{\frac{1}{D}\sum_{i=1}^{D} x_i^2}) - \exp(\frac{1}{D}\sum_{i=1}^{D}\cos(2\pi x_i) + 20 + e)$	0	Multimodal, Non-seperable	[-35,35]	D
F_{43}	Penalized	$f(x) = \frac{\pi}{n}\left\{10sin^2(\pi y_i) + \sum_{i=1}^{n-1}(y_i - 1)^2\, X\,[1 + 10sin^2(3\pi y_i + 1)] + (y_n - 1)^2\right\} + \sum_{i=1}^{30} u(x_i, 10{,}100{,}4)$	0	Multimodal, Non-seperable	[-50,50]	30
F_{44}	Penalized2	$f(x) = 0.1\{sin^2(3\pi x_1) + \sum_{i=1}^{29}(x_i - 1)^2 p\,[1 + sin^2(3\pi x_{i+1})] + (x_n - 1)^2[1 + sin^2(2\pi x_{30})]\} + \sum_{i=1}^{30} u(x_i, 5{,}100{,}4)$	0	Multimodal, Non-seperable	[-50,50]	30

TABLE 11. Benchmark functions (F_{45}-F_{50}).

No	Function Name	Formula	F_{opt}	Type	Range	D
F_{45}	Langerman2	$f(x) = -c_i(\exp(\frac{1}{\pi}\sum_{j=1}^{n}(x_j - a_{ij})^2)\, x\, cos(\pi\sum_{j=1}^{n}(x_j - a_{ij})^2))$	1.08	Multimodal, Non-seperable	[0,10]	2
F_{46}	Langerman5	$f(x) = -c_i(\exp(\frac{1}{\pi}\sum_{j=1}^{n}(x_j - a_{ij})^2)\, x\, cos(\pi\sum_{j=1}^{n}(x_j - a_{ij})^2))$	1.5	Multimodal, Non-seperable	[0,10]	5
F_{47}	Langerman10	$f(x) = -c_i(\exp(\frac{1}{\pi}\sum_{j=1}^{n}(x_j - a_{ij})^2)\, x\, cos(\pi\sum_{j=1}^{n}(x_j - a_{ij})^2))$	-	Multimodal, Non-seperable	[0,10]	10
F_{48}	FletcherPowell2	$A_i = \sum_{j=1}^{n}(a_{ij}sin\alpha_j + b_{ij}cos\alpha_j)$ $B_i = \sum_{j=1}^{n}(a_{ij}sinx_j + b_{ij}cosx_j)$ $f(x) = \sum_{i=1}^{n}(A_i - B_i)^2$	0	Multimodal, Non-seperable	[-π,π]	2
F_{49}	FletcherPowell2	$A_i = \sum_{j=1}^{n}(a_{ij}sin\alpha_j + b_{ij}cos\alpha_j)$ $B_i = \sum_{j=1}^{n}(a_{ij}sinx_j + b_{ij}cosx_j)$ $f(x) = \sum_{i=1}^{n}(A_i - B_i)^2$	0	Multimodal, Non-seperable	[-π,π]	5
F_{50}	FletcherPowell10	$A_i = \sum_{j=1}^{n}(a_{ij}sin\alpha_j + b_{ij}cos\alpha_j)$ $B_i = \sum_{j=1}^{n}(a_{ij}sinx_j + b_{ij}cosx_j)$ $f(x) = \sum_{i=1}^{n}(A_i - B_i)^2$	0	Multimodal, Non-seperable	[-π,π]	10

at threshold 4 with 17.6305, and at threshold 5 with 19.0576. The second average of PSNR values is obtained by AOA at threshold 2 with 12.0833, WOA at threshold 3 and threshold 4 with 15.0239 and 15.7870, and PSO at threshold 5 with 18.5776.

IV. CONCLUSION AND FUTURE WORK

Skin cancer is the most common type of cancer. An early skin cancer diagnosis can significantly reduce the mortality rate. Image segmentation is the first and significant step of image analysis. To develop the classification phase of skin cancer detection, image segmentation plays a critical role by dividing the image into meaningful regions.

Thresholding is one of the most simply established image segmentation methods in the literature.

As the number of thresholds increases, the complexity of the problem increases. To reduce computational times by reducing the complexity of the multilevel thresholding problem, metaheuristic methods are used. This study proposes a particle swarm with a visit table strategy optimization method to determine the best thresholds for skin image segmentation. An efficient and improved version of the original PSO is proposed to solve a few drawbacks of the PSO method. Firstly, the movement equations are updated to avoid stacking into the local optimum. Secondly, it is aimed to ensure that the particles go to places that are not visited first and to discover different points with the visit table strategy. To evaluate the proposed method, two different datasets have been used. Firstly, it is applied to benchmark problems and compared results with seven other metaheuristic methods: AOA, GWO, MFO, WOA, MVO, TLBO, and original PSO. The methods are compared in terms of mean, standard deviation, minimum, and maximum values.

In addition to quantitative and qualitative analysis of the proposed method, the scalability analysis is also performed.

The experimental results confirmed that the IPSO optimization method outperformed the original PSO and other state-of-the-art methods at most of the benchmark functions. Secondly, the proposed method is applied to multilevel thresholding segmentation of skin cancer. The experimental results of the segmentation show that the proposed method

TABLE 12. Comparisons of optimization results for 50 test functions (F1-F6).

Fun.	Index	IPSO	PSO	AOA	GWO	MFO	WOA	MVO	TLBO
F1	Avg	-5	-3.5333	8.6333	-5	-5	-5	-5	-5
	Min	-5.0000	-5.0000	3.0000	-5	-5	-5	-5	-5
	Max	-3.0000	6.0000	13.000	-5	-5	-5	-5	-5
	std	0.5683	3.8032	2.9300	0	0	0	0	0
F2	Avg	0	7.07e+03	0	0	5.00e+03	0	9.5000	0
	Min	0	37	0	0	0	0	3.0000	0
	Max	0	20088	0	0	3.00e+3	0	19.0000	0
	std	0	7.49e+03	0	0	7.76e+03	0	4.0322	0
F3	Avg	3.1e-315	2.27e+03	3.81e-56	4.32e-50	3.33e+03	2.0e-128	0.4774	3.5e-190
	Min	0	5.0114	1.1e-199	1.91e-52	7.63e-05	4.3e-150	0.2192	1.3e-194
	Max	5.3e-314	1.20e+04	5.93e-55	2.30e-49	2.00e+04	5.1e-127	0.9875	4.9e-189
	std	0	4.14e+03	1.45e-55	6.15e-50	6.60e+03	9.4e-128	0.1645	0
F4	Avg	4.7e-316	2.05e+03	0	1.42e-50	823.3427	1.6e-132	0.4547	5.9e-191
	Min	0	88.8946	0	4.49e-53	1.38e-05	4.5e-148	0.0564	7.2e-198
	Max	8.9e-315	4.70e+03	0	2.72e-49	3.10e+03	4.7e-131	1.6233	1.4e-189
	std	0	1.24e+03	0	4.92e-50	882.6575	8.6e-132	0.3893	0
F5	Avg	1.01e-04	131.0287	6.35e-05	0.0013	3.5495	0.0029	0.0274	5.07e-04
	Min	4.74e-06	77.1300	1.11e-06	2.75e-04	0.1251	6.82e-05	0.0150	2.04e-04
	Max	3.03e-04	163.0616	1.87e-04	0.0025	19.1157	0.0223	0.0662	8.63e-04
	std	8.27e-05	25.4226	5.81e-05	4.88e-04	4.9027	0.0051	0.0121	1.73e-04
F6	Avg	3.88e-07	0	0.1832	7.51e-08	0.0254	0.0508	0.2032	0
	Min	3.26e-15	0	0.0000	4.99e-09	0	4.92e-15	0.0000	0
	Max	5.02e-06	0	0.6775	4.69e-07	0.7621	0.7621	0.7621	0
	std	9.52e-07	0	0.2941	9.87e-08	0.1391	0.1933	0.3428	0

outperformed other algorithms in terms of SSIM, FSIM, and PSNR indices.

The novelties of this study are;

- ➢ A visit table strategy and a multiple-direction search strategy are integrated into the algorithm, which prevents unnecessary searches of the PSO algorithm by allowing the discovery of new points with fewer visits to frequently visited points and the neighbors of these points.
- ➢ A multi-level thresholding method based on the proposed PS-VTS optimization algorithm using Renyi's entropy and non-local means 2d-histogram is proposed.

The significant results of the study are given in Table 7. The achievements and advantages of this study are also given as follows:

- ➢ By improving the PSO method with multiple direction search and visit table strategies, significant superiority is achieved over well-known metaheuristic methods in a detailed analysis of the benchmark functions and multi-level segmentation applications.
- ➢ In the qualitative analysis performed on the benchmark functions, the improved PSO algorithm achieved the fastest convergence for unimodal and multimodal functions compared to common metaheuristic methods such as AOA, WOA, GWO, MVO, MFO, TLBO, and PSO
- ➢ In the quantitative analysis performed on the benchmark functions, the proposed optimization method has found more successful results than the other methods according to the average value of 60%, minimum value of 62%, maximum value of 42%, standard deviation value of 46% of the applied 50 test functions.
- ➢ The proposed method is also evaluated against other algorithms with problems of different sizes. In the scalability analysis performed on the benchmark functions, regarding the 10 dimensions, the proposed method ranked first in 10 and second in 5 of the 25 functions, while in the standard deviation values, it ranked first in 10 and second in 7 of the functions. In 50 dimensions, the proposed method ranked first in 12 and second in 5 of the 25 functions, while in the standard deviation values, it ranked first in 12 and second in 11 of the functions. Finally, regarding the 100 dimensions, improved PSO achieved the best average and best standard deviation in 14 and 7 test functions, respectively.
- ➢ In the multilevel thresholding skin cancer image segmentation, the proposed optimization algorithm outperforms the other algorithms for nearly all threshold levels and images.
- ➢ According to the average values of the evaluation metrics for all images, the best results in SSIM value of 0.8285, FSIM value of 0.7332, and PSNR value of 19.0576 are achieved by using the proposed method in skin cancer image segmentation.
- ➢ This study also provides a detailed analysis of well-known metaheuristic approaches for multi-level thresholding image segmentation applications and benchmark problems with quantitative, qualitative, and scalability analysis.

TABLE 13. Comparisons of optimization results for 50 test functions (F7-F21).

Fun.	Index	IPSO	PSO	AOA	GWO	MFO	WOA	MVO	TLBO
F7	Avg	-1.0000	-1	-0.1667	-1.0000	-1	-0.9667	-0.9000	-1
	Min	-1.0000	-1	-1.0000	-1.0000	-1	-1.0000	-1.0000	-1
	Max	-1.0000	-1	-0.0001	-1.0000	-1	0	0	-1
	std	1.54e-14	0	0.3790	0.0000	0	0.1826	0.3051	0
F8	Avg	2.2e-319	8.03e-89	0	7.2e-160	1.1e-32	0	1.1e-08	5.5e-271
	Min	0	1.3e-103	0	3.3e-184	4.3e-75	0	1.61e-10	1.8e-289
	Max	5.5e-318	2.40e-87	0	2.1e-158	3.3e-31	9.8e-324	7.6e-08	1.6e-269
	std	0	4.38e-88	0	3.9e-159	6.06e-32	0	1.58e-08	0
F9	Avg	0.0643	1.1500	0.4688	2.4916	1.7948	1.5874	0.0123	5.04e-09
	Min	2.15e-09	1.31e-04	0.0107	0.0001	7.68e-04	0.0083	5.94e-05	9.03e-13
	Max	0.5465	7.8700	3.9235	7.1185	7.8603	8.2480	0.1068	3.87e-08
	std	0.1361	1.9765	0.7203	2.5150	2.3214	2.5747	0.0215	1.06e-08
F10	Avg	-49.8296	-44.4000	18.1345	-49.9999	-50.0000	-49.9996	-49.9999	-50.0000
	Min	-50.0000	-50.0000	13.9631	-50.0000	-50.0000	-50.0000	-50.0000	-50.0000
	Max	-48.7582	118.0000	20.6252	-49.9997	-50.0000	-49.9971	-49.9994	-50.0000
	std	0.3104	30.6725	1.3642	0.0001	4.55e-12	0.0006	1.13e-04	2.08e-13
F11	Avg	-140.402	-34.0448	6.5312	-164.122	90.5697	-209.839	-209.944	-209.953
	Min	-197.878	-210.000	-0.5679	-209.997	-209.998	-209.992	-209.998	-210.000
	Max	-75.4329	1.98e+03	12.6303	-45.0243	3.53e+03	-209.375	-209.567	-209.793
	std	35.2272	508.1316	3.0399	55.9518	810.2896	0.1548	0.1007	0.0444
F12	Avg	1.2e-314	5.6002	52.9450	7.68e-55	16.5318	2.9781	2.91e-04	4.9e-110
	Min	0	3.58e-20	32.1837	9.87e-63	1.47e-14	0.0002	6.76e-05	2.5e-116
	Max	3.7e-313	42.8892	75.6941	2.23e-53	80.2102	16.8227	7.53e-04	1.2e-108
	std	0	12.4044	9.5404	4.06e-54	19.7914	4.3690	1.89e-04	2.2e-109
F13	Avg	1.0e-311	549.5404	0.0244	4.11e-06	687.1879	6.62e-06	0.5944	3.24e-07
	Min	0	8.0892	2.84e-83	5.29e-08	0.0145	1.33e-30	0.1513	1.59e-13
	Max	2.0e-310	5.36e+03	0.6684	2.72e-05	3.78e+03	3.90e-05	1.4422	6.00e-06
	std	0	1.15e+03	0.1218	5.89e-06	1.02e+03	1.07e-05	0.3271	1.10e-06
F14	Avg	1.5e-156	25.1983	0	1.55e-29	33.0007	5.39e-94	0.6146	7.95e-96
	Min	1.1e-175	6.8600	0	2.64e-30	4.31e-04	3.7e-108	0.2394	1.10e-97
	Max	4.6e-155	45.1777	0	5.80e-29	110.0000	1.38e-92	1.3122	7.58e-95
	std	8.5e-156	11.2633	0	1.44e-29	25.0718	2.54e-93	0.2457	1.51e-95
F15	Avg	2.6e-319	2.03e+04	0.0031	1.69e-09	1.79e+04	2.99e+04	88.8993	5.36e-44
	Min	0	4.45e+03	0.0000	1.30e-16	1.47e+03	4.64e+03	36.8332	2.95e-51
	Max	6.6e-318	4.07e+04	0.0199	3.52e-08	4.17e+04	5.57e+04	165.7206	1.47e-42
	std	0	8.56e+03	0.0057	6.82e-09	1.15e+04	1.14e+04	37.7064	2.68e-43
F16	Avg	28.7223	1.55e+06	28.3168	26.9678	2.68e+06	27.7933	206.5566	25.5933
	Min	28.6993	1.73e+04	27.2311	25.3052	11.7659	26.7619	29.6640	24.7906
	Max	28.7661	5.45e+06	28.8167	28.7650	8.00e+07	28.7783	1.61e+03	26.1739
	std	0.0147	1.61e+06	0.3814	0.8987	1.46e+07	0.6644	335.3382	0.3127
F17	Avg	0.9665	1.05e+04	0.6667	0.6667	4.93e+04	0.6668	3.0067	0.6667
	Min	0.8550	253.0600	0.6667	0.6667	0.0423	0.6667	0.7225	0.6667
	Max	0.9923	8.86e+04	0.6667	0.6667	3.91e+05	0.6670	17.4054	0.6667
	std	0.0330	1.73e+04	0.0000	1.23e-06	9.17e+04	1.11e-04	4.0463	4.32e-12
F18	Avg	2.0496	3.1665	7.6813	5.1662	4.2444	2.9997	0.9980	0.9980
	Min	0.9980	0.9980	0.9980	0.9980	0.9980	0.9980	0.9980	0.9980
	Max	12.6705	9.8039	12.6705	12.6705	20.1535	10.7632	0.9980	0.9980
	std	3.1209	2.5963	4.8188	4.8147	5.1031	2.7911	1.09e-11	0
F19	Avg	0.3981	0.4494	0.4011	0.3979	0.3979	0.3979	0.3979	0.3979
	Min	0.3979	0.3979	0.3980	0.3979	0.3979	0.3979	0.3979	0.3979
	Max	0.3989	1.9431	0.4085	0.3979	0.3979	0.3979	0.3979	0.3979
	std	2.51e-04	0.2821	0.0027	8.87e-07	0	3.87e-06	2.98e-07	0
F20	Avg	0	0	0	0	0	0	1.93e-04	0
	Min	0	0	0	0	0	0	1.06e-05	0
	Max	0	0	0	0	0	0	5.97e-04	0
	std	0	0	0	0	0	0	1.45e-04	0
F21	Avg	1.07e-14	0	4.73e-07	2.63e-07	0	5.49e-04	2.68e-07	0
	Min	2.52e-27	0	1.87e-08	7.26e-11	0	1.08e-05	2.08e-09	0
	Max	2.47e-13	0	1.93e-06	1.13e-06	0	0.0017	1.04e-06	0
	std	4.54e-14	0	4.93e-07	2.87e-07	0	5.02e-04	2.44e-07	0

TABLE 14. Comparisons of optimization results for 50 test functions (F22-F36).

Fun.	Index	IPSO	PSO	AOA	GWO	MFO	WOA	MVO	TLBO
F22	Avg	0	171.5601	0	0.6800	180.4420	1.89e-15	118.677	14.1645
	Min	0	103.9156	0	0	98.5005	0	63.9350	1.5721
	Max	0	283.1658	0	8.8993	259.8960	5.68e-14	210.228	33.0903
	std	0	43.6998	0	1.9056	35.6430	1.03e-14	37.9570	6.2158
F23	Avg	-4.4e+03	-6.9e+03	-6707.6	-5.9e+03	-8.3e+03	-1.0e+04	-7.9e+03	-7.7e+03
	Min	-5.2e+03	-9.4e+03	-8202.2	-7.8e+03	-9.7e+03	-1.2e+04	-9.3e+03	-8.7e+03
	Max	-3.8e+03	-5.0e+03	-5898.7	-3.2e+03	-6.4e+03	-6.5e+03	-6.7e+03	-6.6e+03
	std	365.4246	1.12e+03	447.2	882.6682	843.1291	1.91e+03	671.893	538.4442
F24	Avg	-1.8013	-1.8013	-1.7945	-1.7746	-1.8013	-1.8013	-1.8013	-1.8013
	Min	-1.8013	-1.8013	-1.8007	-1.8013	-1.8013	-1.8013	-1.8013	-1.8013
	Max	-1.8013	-1.8013	-1.7724	-1.0000	-1.8013	-1.8013	-1.8013	-1.8013
	std	6.23e-09	9.19e-16	0.0062	0.1463	9.03e-16	1.17e-06	2.28e-07	9.03e-16
F25	Avg	-4.2681	-4.1985	-3.2513	-4.1501	-4.2334	-3.5471	-3.9627	-4.5370
	Min	-4.6877	-4.6877	-3.8107	-4.6876	-4.6877	-4.4949	-4.6459	-4.6877
	Max	-3.8731	-2.7773	-2.6082	-2.8446	-3.3749	-2.2982	-3.2902	-3.8446
	std	0.1489	0.4875	0.2774	0.5130	0.3974	0.6365	0.44950	0.1509
F26	Avg	-6.0300	-7.5340	-4.5775	-7.5681	-7.7196	-5.7288	-6.9424	-8.9293
	Min	-7.0597	-9.1715	-5.7824	-9.2981	-9.3834	-7.8537	-8.3165	-9.6135
	Max	-5.3617	-4.0719	-3.7992	-5.8670	-3.9069	-3.5932	-5.1014	-7.2023
	std	0.4033	1.0869	0.4405	0.8355	1.1696	0.8569	0.92480	0.4817
F27	Avg	0	0	0	0	0.0007	0	1.41e-08	0
	Min	0	0	0	0	0	0	3.98e-10	0
	Max	0	0	0	0	0.0094	0	5.38e-08	0
	std	0	0	0	0	0.0020	0	1.47e-08	0
F28	Avg	-1.0316	-1.0316	-1.0316	-1.0316	-1.0316	-1.0316	-1.0316	-1.0316
	Min	-1.0316	-1.0316	-1.0316	-1.0316	-1.0316	-1.0316	-1.0316	-1.0316
	Max	-1.0315	-1.0316	-1.0316	-1.0316	-1.0316	-1.0316	-1.0316	-1.0316
	std	1.50e-05	6.25e-16	1.04e-07	9.17e-09	6.77e-16	3.75e-10	1.51e-07	6.71e-16
F29	Avg	0	0	0	0	0	0	2.03e-04	0
	Min	0	0	0	0	0	0	7.36e-06	0
	Max	0	0	0	0	0	0	5.86e-04	0
	std	0	0	0	0	0	0	1.82e-04	0
F30	Avg	0	0	0	0	0	7.06e-16	6.39e-05	0
	Min	0	0	0	0	0	0	5.01e-07	0
	Max	0	0	0	0	0	5.16e-15	2.91e-04	0
	std	0	0	0	0	0	1.11e-15	6.98e-05	0
F31	Avg	-186.730	-186.730	-148.411	-186.713	-186.730	-186.730	-186.730	-186.730
	Min	-186.730	-186.730	-186.730	-186.730	-186.730	-186.730	-186.730	-186.730
	Max	-186.265	-186.730	-64.4039	-186.509	-186.730	-186.725	-186.729	-186.730
	std	0.1161	9.20e-14	43.9930	0.0564	3.42e-14	0.0012	2.88e-04	5.70e-14
F32	Avg	3.0000	8.4000	6.1828	5.7000	3.0000	3.0000	5.7000	3.0000
	Min	3.0000	3.0000	3.0000	3.0000	3.0000	3.0000	3.0000	3.0000
	Max	3.0000	84.0000	52.3316	84.0000	3.0000	3.0006	84.000	3.0000
	std	3.92e-12	20.5504	10.2223	14.7885	1.97e-15	0.0001	14.788	5.53e-16
F33	Avg	3.25e-04	0.0032	0.0108	0.0044	0.0029	0.0007	0.0078	3.24e-04
	Min	3.07e-04	0.0003	0.0003	0.0003	0.0006	0.0003	0.0003	3.07e-04
	Max	5.11e-04	0.0204	0.0983	0.0204	0.0204	0.0030	0.0204	8.11e-04
	std	4.13e-05	0.0060	0.0223	0.0081	0.0051	0.0006	0.0094	9.19e-05
F34	Avg	-10.1092	-5.8020	-4.8968	-8.9014	-5.2979	-8.8752	-7.7191	-9.5343
	Min	-10.1532	-10.1532	-8.6498	-10.1531	-10.1532	-10.1531	-10.153	-10.1532
	Max	-9.9756	-2.6305	-3.0341	-3.0653	-2.6305	-2.6299	-2.6305	-2.6305
	std	0.0518	3.0765	1.3241	2.3326	2.9285	2.6183	3.12960	1.7678
F35	Avg	-10.2468	-6.4679	-5.4107	-10.4023	-6.8348	-7.9980	-8.0523	-9.6712
	Min	-10.4029	-10.4029	-8.4493	-10.4029	-10.4029	-10.5358	-10.402	-10.4029
	Max	-9.5082	-1.8376	-3.4310	-10.4013	-2.7519	-1.6738	-2.7519	-4.3973
	std	0.2387	3.6121	1.4997	0.0004	3.4617	3.0047	3.00050	1.9007
F36	Avg	-10.5359	-5.5773	-5.3862	-10.5359	-7.8874	-7.5377	-8.5822	-10.3216
	Min	-10.5364	-10.5364	-8.0426	-10.5363	-10.5364	-10.5356	-10.536	-10.5364
	Max	-8.2170	-1.8595	-2.3074	-10.5352	-2.4217	-2.4262	-2.4273	-4.0925
	std	0.6867	3.6336	1.2916	0.002	3.3614	3.3260	3.11650	1.1765

Future studies can be expanded in two directions: the first one is aimed at further improving the segmentation effectiveness of skin cancer images. In this context, it is aimed to investigate the effectiveness of different objective functions (fuzzy transforms, energy curve, Kapur's entropy, Tasallis entropy, minimum cross-entropy), to find the threshold

TABLE 15. Comparisons of optimization results for 50 test functions (F37-F50).

Fun.	Index	IPSO	PSO	AOA	GWO	MFO	WOA	MVO	TLBO
F37	Avg	3.1350	30.1130	75.7100	2.0926	0.2935	12.2489	0.0941	0.0251
	Min	0.4450	0.0014	1.9080	0.0028	1.31e-04	0.0746	1.89e-04	1.47e-05
	Max	8.2511	895.5317	511.1259	11.2273	2.4321	221.4849	0.4729	0.4537
	std	2.0273	163.4523	128.7612	2.4556	0.6018	40.2212	0.1594	0.0831
F38	Avg	0.0352	0.0153	0.1602	0.3336	0.0734	4.1071	0.0010	0.0003
	Min	0.0033	0.0002	0.0068	2.26e-04	1.05e-05	0.0391	3.19e-05	1.15e-07
	Max	0.1206	0.0878	0.6145	0.8864	0.8875	21.1317	0.0045	0.0029
	std	0.0286	0.0226	0.1426	0.3793	0.2218	5.6754	0.0013	0.0005
F39	Avg	-3.8628	-3.8628	-3.8552	-3.8613	-3.8628	-3.8565	-3.8628	-3.8628
	Min	-3.8628	-3.8628	-3.8621	-3.8628	-3.8628	-3.8628	-3.8628	-3.8628
	Max	-3.8628	-3.8628	-3.8491	-3.8549	-3.8628	-3.8171	-3.8628	-3.8628
	std	3.16e-08	2.62e-15	0.0027	0.0026	2.71e-15	0.0104	8.11e-07	2.69e-15
F40	Avg	-3.3094	-3.1812	-3.1406	-3.2592	-3.2194	-3.2359	-3.2619	-3.3092
	Min	-3.3220	-3.3220	-3.2476	-3.3220	-3.3220	-3.3219	-3.3220	-3.3220
	Max	-3.2550	-1.7061	-3.0079	-3.0784	-3.1345	-2.8397	-3.1998	-3.2031
	std	0.0183	0.2884	0.0540	0.0832	0.0624	0.1208	0.0611	0.0340
F41	Avg	0	30.3606	0.1572	0.0055	21.0908	0.0065	0.7050	0
	Min	0	3.3841	0.0167	0	0.0001	0	0.5337	0
	Max	0	134.2443	0.3711	0.0361	180.0915	0.1103	0.8772	0
	std	0	35.8234	0.0973	0.0106	45.3859	0.0250	0.0940	0
F42	Avg	8.88e-16	13.5760	8.88e-16	2.10e-14	16.9355	3.84e-15	1.5304	6.21e-15
	Min	8.88e-16	8.4883	8.88e-16	1.50e-14	2.2201	8.88e-16	0.2018	4.44e-15
	Max	8.88e-16	20.6453	8.88e-16	2.93e-14	19.9627	7.99e-15	3.4260	7.99e-15
	std	0	3.3273	0	3.88e-15	5.4583	2.30e-15	0.7873	1.80e-15
F43	Avg	0.0349	3.16e+05	0.4712	0.0563	3.43e+03	0.0323	1.8216	0.0104
	Min	0.0110	12.1928	0.3896	0.0202	6.40e-04	0.0032	0.0401	7.58e-11
	Max	0.1719	4.12e+06	0.5734	0.1118	1.03e+05	0.4687	5.1553	0.1037
	std	0.0333	8.64e+05	0.0472	0.0229	1.88e+04	0.0830	1.1358	0.0316
F44	Avg	0.3807	8.51e+04	2.8030	0.6971	43.0455	0.5046	0.1175	0.0792
	Min	0.1624	58.2666	2.6257	0.2222	0.0320	0.0872	0.0418	5.05e-08
	Max	1.3960	9.39e+05	2.9619	1.1336	530.3682	1.4896	0.2949	0.2932
	std	0.2638	2.10e+05	0.0836	0.2487	110.7600	0.3087	0.0591	0.0744
F45	Avg	-1.0809	-1.0759	-1.0790	-1.0809	-1.0734	-1.0764	-1.0809	-1.0809
	Min	-1.0809	-1.0809	-1.0809	-1.0809	-1.0809	-1.0809	-1.0809	-1.0809
	Max	-1.0809	-1.0053	-1.0738	-1.0809	-1.0053	-0.9456	-1.0809	-1.0809
	std	1.32e-06	0.0192	0.0019	2.27e-07	0.0231	0.0247	3.73e-07	4.51e-16
F46	Avg	-1.3996	-0.8585	-0.9043	-1.0598	-0.8202	-0.6155	-1.2173	-1.1506
	Min	-1.5000	-1.5000	-1.3465	-1.5000	-1.5000	-0.9175	-1.5000	-1.5000
	Max	-1.0119	-0.2233	-0.5276	-0.5056	-0.4502	-0.1352	-0.9080	-0.4829
	std	0.1390	0.3677	0.2032	0.3181	0.3430	0.1873	0.2878	0.3810
F47	Avg	-0.5679	-0.2951	-0.2909	-0.4483	-0.3699	-0.1808	-0.5258	-0.4100
	Min	-0.7977	-0.7977	-0.5352	-0.7977	-0.7977	-0.4829	-0.8760	-0.7977
	Max	-0.2447	-0.0215	-0.0800	-0.1455	-0.0199	-0.0279	-0.2749	-0.1181
	std	0.2151	0.1732	0.1098	0.2312	0.2370	0.1262	0.1765	0.1882
F48	Avg	0.0051	23.5098	3.13e-05	23.5187	0	2.09e-07	90.3130	0
	Min	5.47e-06	0	1.31e-07	3.05e-05	0	7.85e-11	5.18e-07	0
	Max	0.0189	705.2950	1.87e-04	705.2950	0	1.30e-06	1.29e+03	0
	std	0.0053	128.7687	3.61e-05	128.7670	0	3.85e-07	289.8909	0
F49	Avg	31.3898	939.7024	8.13e+03	188.1204	220.2955	375.8342	374.3277	33.6348
	Min	4.59e-04	9.4437	0.0172	0.0708	5.65e-26	0.4913	0.0017	2.01e-28
	Max	130.8601	3.55e+03	4.38e+04	1.50e+03	2.07e+03	2.28e+03	3.60e+03	185.9625
	std	34.7920	1.26e+03	1.02e+04	277.8448	453.8911	706.5158	823.0286	69.7259
F50	Avg	1.06e+04	1.23e+04	1.31e+05	4.78e+03	4.51e+03	1.33e+04	2.96e+03	2.09e+03
	Min	555.7501	9.4277	3.22e+04	108.1057	196.4413	300.4677	1.8504	0.1457
	Max	2.41e+04	7.85e+04	2.17e+05	2.96e+04	1.10e+04	4.47e+04	3.34e+04	1.47e+04
	std	6.53e+03	2.21e+04	4.66e+04	6.64e+03	3.51e+03	1.38e+04	6.59e+03	3.21e+03

number adaptively based on the image by using these objective functions [12], and to perform color image segmentation based on various histograms.

Secondly, the logic of preventing unnecessary searches by creating a memory matrix with the visit table strategy will be used to eliminate the deficiencies of various metaheuristics

TABLE 16. The comparison results of all algorithms with Dim = 10 & 50 using 50 Benchmark functions (F1-F10).

Fun.	Dim	Index	IPSO	PSO	AOA	GWO	MFO	WOA	MVO	TLBO
F1	D=10	Avg	-2.3333	-5	8.3333	-4.6667	-5	-5	-5	-5
		Std	0.6609	0	2.4960	1.2685	0	0	0	0
	D=50	Avg	-2.5000	-5	9.5333	-4.8333	-5	-5	-5	-5
		Std	0.5724	0	2.0965	0.9129	0	0	0	0
	D=100	Avg	-2.4000	-5	8.2000	-4.8333	-5	-5	-5	-5
		Std	0.5632	0	2.8089	0.9129	0	0	0	0
F2	D=10	Avg	0	9.7667	0	0	0	0.0333	0.7000	0
		Std	0	19.6006	0	0	0	0.1826	0.8367	0
	D=50	Avg	0	1.72e+04	0	0	8.4470	0.0333	35.4333	0
		Std	0	6.57e+03	0	0	6.7275	0.1826	12.4670	0
	D=100	Avg	0	7.11e+04	0	0	4.53e+04	0.0333	256.8667	0
		Std	0	1.12e+04	0	0	1.67e+04	0.1826	56.4524	0
F3	D=10	Avg	1.3e-296	1.22e-07	0	1.01e-96	4.24e-28	0.0733	0.0061	0.5876
		Std	0	6.72e-07	0	3.07e-96	1.08e-27	0.4008	0.0032	0
	D=50	Avg	4.0e-280	1.57e+04	1.94e-04	3.75e-37	6.6944	7.8e-127	3.8839	7.7e-183
		Std	0	6.46e+03	6.08e-04	8.64e-37	7.5064	3.0e-126	1.2619	0
	D=100	Avg	1.1e-275	6.77e+04	0.0211	2.10e-25	3.69e+04	6.2e-125	63.9135	7.3e-176
		Std	0	1.34e+04	0.0093	2.31e-25	1.44e+04	3.4e-124	10.8436	0
F4	D=10	Avg	1.1e-290	3.3333	0	2.26e-99	1.28e-29	0.1385	7.11e-04	0.1751
		Std	0	18.2574	0	8.05e-99	3.31e-29	0.7585	8.96e-04	0
	D=50	Avg	2.9e-290	3.81e+03	0	6.34e-38	2.76e+03	2.3e-128	10.5261	3.7e-183
		Std	0	1.43e+03	0	8.50e-38	2.38e+03	1.0e-127	9.1887	0
	D=100	Avg	2.1e-289	3.21e+04	5.4e-104	8.79e-26	1.92e+04	1.9e-125	167.7989	1.3e-176
		Std	0	6.79e+03	2.9e-103	1.02e-25	8.42e+03	9.8e-125	64.5524	0
F5	D=10	Avg	3.70e-04	0.0235	5.33e-04	5.20e-04	0.0135	0.0015	0.0026	0.3865
		Std	3.56e-04	0.0173	6.00e-04	3.20e-04	0.0114	0.0021	0.0018	0.1854
	D=50	Avg	3.66e-04	19.9504	4.96e-04	0.0020	23.1602	0.0028	0.0875	6.37e-04
		Std	3.60e-04	10.7591	5.08e-04	0.0012	22.6582	0.0025	0.0277	2.04e-04
	D=100	Avg	3.89e-04	215.7756	4.83e-04	0.0039	228.8346	0.0030	0.4554	7.73e-04
		Std	3.82e-04	69.3645	3.91e-04	0.0013	161.9823	0.0032	0.1043	2.84e-04
F6	D=10	Avg	4.77e-17	0.1524	0.2237	0.0762	2.78e-12	0.0762	0.2032	0
		Std	2.45e-16	0.3100	0.3150	0.2325	1.21e-18	0.2325	0.3428	0
	D=50	Avg	2.26e-16	0.0254	0.0897	0.0762	4.09e-10	0.0254	0.0254	0
		Std	9.22e-16	0.1391	0.2318	0.2325	2.24e-09	0.1391	0.1391	0
	D=100	Avg	0.0508	0.0508	0.1423	0.0762	5.96e-19	0.1016	0.1778	0.0254
		Std	0.1933	0.1933	0.3465	0.2325	2.63e-18	0.2635	0.3278	0.1391
F7	D=10	Avg	-1	-0.9667	-0.1667	-1	-1	-1	-0.7667	-1
		Std	5.31e-13	0.1826	0.3790	2.98e-07	0	2.25e-05	0.4302	0
	D=50	Avg	-1	-1	-0.0667	-1	-1	-1	-0.7667	-1
		Std	7.60e-15	0	0.2537	3.36e-07	0	6.59e-07	0.4302	0
	D=100	Avg	-1	-1	-0.1692	-1	-1	-1	-0.8666	-1
		Std	1.46e-14	0	0.3781	3.16e-07	0	9.25e-07	0.3457	0
F8	D=10	Avg	7.9e-299	1.93e-91	0	1.2e-165	1.85e-27	0	1.38e-08	0.3711
		Std	0	7.66e-91	0	0	1.00e-26	0	1.55e-08	0
	D=50	Avg	2.1e-286	9.33e-88	0	4.0e-156	9.17e-24	0	1.31e-08	3.8e-272
		Std	0	5.09e-87	0	2.1e-155	4.60e-23	0	1.50e-08	0
	D=100	Avg	1.6e-289	6.80e-89	0	2.1e-161	1.03e-31	0	1.21e-08	5.9e-271
		Std	0	3.72e-88	0	1.0e-160	5.68e-31	0	1.37e-08	0
F9	D=10	Avg	0.5163	0.6118	0.4107	1.7882	1.1481	1.1174	0.0288	2.28e-08
		Std	0.8427	1.2964	0.2929	2.2618	1.6452	1.5756	0.0361	7.09e-08
	D=50	Avg	0.6659	0.5901	0.5392	2.3383	1.4443	1.4550	0.2809	2.25e-09
		Std	1.0807	1.4361	0.6075	2.5790	2.0132	2.3931	1.4325	1.02e-08
	D=100	Avg	0.7388	0.6205	0.6441	1.5464	1.4387	1.9652	0.0945	7.11e-09
		Std	1.1869	1.3116	0.9473	2.0716	2.0454	2.4146	0.3795	1.85e-08
F10	D=10	Avg	-34.7300	-50	-25.4844	-49.2987	-41.1000	-49.9997	-49.9999	-50.0000
		Std	9.8948	1.78e-12	5.1730	3.8403	48.7473	3.25e-04	9.32e-05	2.56e-13
	D=50	Avg	-30.7602	-44.4000	-26.4680	-49.9998	-50	-49.9997	-49.9998	-50.0000
		Std	10.5854	30.6725	4.8359	8.88e-05	2.15e-11	3.53e-04	1.29e-04	1.54e-13
	D=100	Avg	-32.7500	-35.4999	-27.4154	-49.9999	-43.6000	-49.9996	-49.9999	-50.0000
		Std	9.5395	56.6920	3.4636	1.04e-04	35.0542	4.00e-04	1.25e-04	1.13e-13

and strengthen the methods. In addition, by performing searches in all directions with a multiple-direction search strategy, the algorithms will be improved by increasing their exploration abilities and eliminating their deficiencies.

TABLE 17. The comparison results of all algorithms with Dim = 10 & 50 using 50 Benchmark functions (F11-F20).

Fun.	Dim	Index	IPSO	PSO	AOA	GWO	MFO	WOA	MVO	TLBO
F11	D=10	Avg	-70.0894	13.1355	-33.4225	-164.627	67.4598	-209.870	-209.9692	-209.952
		Std	30.7333	742.3823	5.0589	55.1747	523.8394	0.1802	0.0311	0.0445
	D=50	Avg	-74.7791	-155.3141	-32.7910	-146.365	-209.7237	-209.856	-209.9577	-209.967
		Std	33.5064	240.7727	5.3491	63.6424	0.3335	0.1384	0.0438	0.0423
	D=100	Avg	-67.5101	-184.3951	-36.7645	-177.739	130.3926	-209.816	-209.9611	-209.960
		Std	25.6536	70.1154	9.2187	50.1468	592.3856	0.1675	0.0511	0.0468
F12	D=10	Avg	1.4e-296	13.1303	1.00e-06	3.55e-56	35.0192	4.3319	3.59e-04	3.7e-109
		Std	0	29.4169	5.48e-06	1.21e-55	38.2265	5.0470	2.55e-04	1.7e-108
	D=50	Avg	2.3e-288	8.6259	2.27e-07	9.95e-57	23.9583	7.3461	2.90e-04	1.0e-108
		Std	0	20.8923	1.00e-06	3.20e-56	26.4745	13.6225	1.48e-04	5.6e-108
	D=100	Avg	5.6e-286	2.2053	1.81e-05	7.86e-57	20.8409	2.7743	3.29e-04	2.9e-110
		Std	0	5.5525	9.84e-05	2.73e-56	30.2921	4.0925	1.69e-04	1.2e-109
F13	D=10	Avg	3.9e-290	558.2056	0.0013	3.29e-06	988.3778	3.48e-06	0.4527	2.11e-07
		Std	0	984.8962	0.0064	2.83e-06	1.37e+03	1.29e-05	0.2700	4.46e-07
	D=50	Avg	4.4e-287	393.0426	0.0414	3.49e-06	694.3744	6.91e-06	0.4301	2.43e-07
		Std	0	823.1159	0.1625	4.48e-06	1.00e+03	1.82e-05	0.1915	6.19e-07
	D=100	Avg	1.6e-294	513.0564	0.0034	3.16e-06	637.9918	4.29e-06	0.4890	2.17e-07
		Std	0	914.4187	0.0117	3.90e-06	835.2626	1.25e-05	0.2542	5.20e-07
F14	D=10	Avg	4.0e-146	0.4963	0	2.42e-56	2.3333	4.22e-97	0.0241	1.1e-114
		Std	2.2e-145	1.9385	0	3.76e-56	4.3018	2.29e-96	0.0078	2.0e-114
	D=50	Avg	3.2e-146	73.9335	3.4e-259	2.34e-22	53.8982	4.90e-94	4.28e+04	1.89e-92
		Std	1.7e-145	22.5755	0	2.53e-22	26.2740	2.63e-93	2.34e+05	3.32e-92
	D=100	Avg	9.5e-145	9.37e+09	8.05e-87	1.27e-15	181.9600	9.46e-94	2.59e+21	9.14e-90
		Std	5.0e-144	5.13e+10	4.35e-86	8.21e-16	45.2704	3.89e-93	1.42e+22	9.33e-90
F15	D=10	Avg	1.9e-283	208.6702	1.2e-119	8.67e-43	888.8890	49.5760	0.0524	1.2e-101
		Std	0	912.0898	6.6e-119	2.43e-42	2.04e+03	85.8743	0.0448	5.2e-101
	D=50	Avg	2.8e-284	6.25e+04	0.0748	0.0010	5.57e+04	1.84e+05	3.18e+03	9.29e-31
		Std	0	1.79e+04	0.1255	0.0022	2.19e+04	3.65e+04	998.8557	4.35e-30
	D=100	Avg	1.9e-308	2.32e+05	0.7069	29.3191	2.21e+05	1.00e+06	5.47e+04	9.29e-21
		Std	0	4.49e+04	0.4713	35.1778	5.97e+04	2.08e+05	6.46e+03	4.43e-20
F16	D=10	Avg	8.9242	3.15e+03	6.2812	6.7193	6.26e+03	6.7124	118.2874	3.2970
		Std	0.0260	1.64e+04	0.2954	0.5445	2.27e+04	0.8250	340.9739	0.8030
	D=50	Avg	48.6082	1.43e+07	48.6746	47.1933	1.38e+07	47.8230	793.9512	46.2593
		Std	0.0893	7.78e+06	0.2040	0.7775	3.67e+07	0.4831	826.3983	0.6146
	D=100	Avg	98.1460	1.26e+08	98.8237	97.9336	1.10e+08	97.9760	3.99e+03	96.8729
		Std	0.0369	4.23e+07	0.1542	0.5477	7.07e+07	0.4197	3.11e+03	0.8308
F17	D=10	Avg	0.8952	1.0442	0.6667	0.6667	20.0810	0.6526	0.6046	0.6667
		Std	0.0552	3.0222	3.62e-09	8.56e-05	36.4546	0.1282	0.1955	6.33e-16
	D=50	Avg	0.9968	2.63e+05	0.6667	0.6667	1.65e+05	0.6667	18.9904	0.6667
		Std	0.0021	1.91e+05	3.85e-07	1.01e-05	2.78e+05	1.03e-04	18.3362	6.08e-09
	D=100	Avg	0.9978	2.65e+06	0.6667	0.6667	3.15e+06	0.6669	166.1779	0.6667
		Std	0.0009	8.02e+05	3.99e-05	4.12e-05	2.16e+06	1.83e-04	83.2397	1.47e-09
F18	D = 10	Avg	5.1993	3.6791	9.7207	4.3958	3.1381	4.7492	0.9980	0.9980
		Std	5.1203	3.6644	4.0575	3.9914	2.0978	4.3943	8.01e-12	0
	D=50	Avg	5.9710	4.3872	7.3392	5.7226	3.5554	3.5744	0.9980	0.9980
		Std	5.5107	4.4955	4.3072	4.7040	3.0977	4.0817	2.18e-11	0
	D=100	Avg	1.0989	4.6187	8.0198	4.0370	2.7974	3.1218	0.9980	0.9980
		Std	0.3992	4.3601	4.7820	3.8813	3.1819	3.5626	1.15e-11	0
F19	D=10	Avg	0.3979	0.4494	0.4011	1.82e-06	0.3979	0.3979	0.3979	0.3979
		Std	3.9e-05	0.2821	0.0028	0.3979	0	1.46e-05	2.46e-07	0
	D=50	Avg	0.3979	0.4494	0.4016	0.3979	0.3979	0.3979	0.3979	0.3979
		Std	3.29e-05	0.2821	0.0024	1.10e-06	0	3.62e-06	1.46e-07	0
	D=100	Avg	0.3979	0.3979	0.4018	0.3979	0.3979	0.3979	0.3979	0.3979
		Std	2.17e-04	0	0.0037	1.41e-04	0	5.19e-06	3.35e-07	0
F20	D=10	Avg	0	0	0	0	0	0	2.21e-04	0
		Std	0	0	0	0	0	0	1.74e-04	0
	D=50	Avg	0	0	0	0	0	0	1.94e-04	0
		Std	0	0	0	0	0	0	1.84e-04	0
	D=100	Avg	0	0	0	0	0	0	2.13e-04	0
		Std	0	0	0	0	0	0	1.73e-04	0

APPENDIX

See Tables 9–18.

DECLARATIONS

Conflict of interest None declared.

TABLE 18. The comparison results of all algorithms with Dim=10&50 using 50 Benchmark functions (F21-F25).

Fun.	Dim	Index	IPSO	PSO	AOA	GWO	MFO	WOA	MVO	TLBO
F21	D=10	Avg	1.85e-08	0	4.90e-07	1.75e-07	0	4.20e-04	2.55e-07	0
		Std	3.68e-08	0	4.62e-07	1.31e-07	0	8.02e-04	1.99e-07	0
	D =50	Avg	1.31e-08	0	3.50e-07	2.06e-07	0	0.0008	3.07e-07	0
		Std	2.60e-08	0	3.47e-07	1.78e-07	0	0.0010	3.37e-07	0
	D=100	Avg	1.95e-08	0	3.99e-07	1.68e-07	0	0.0010	3.14e-07	0
		Std	3.52e-08	0	4.10e-07	1.41e-07	0	0.0014	3.58e-07	0
F22	D =10	Avg	0	24.6983	0	0.1390	27.8374	1.0702	13.7340	2.8150
		Std	0	12.2150	0	0.7615	14.2236	5.8615	5.7625	2.2358
	D = 50	Avg	0	375.1769	0	1.4881	337.1644	0	241.9643	19.1591
		Std	0	66.6017	0	3.2193	63.3558	0	43.5466	22.3274
	D=100	Avg	0	948.2253	0	1.4848	789.5306	3.78e-15	653.0561	5.5207
		Std	0	103.6840	0	3.1858	58.4415	2.07e-14	65.9137	30.2383
F23	D =10	Avg	-2.5e+03	-3.13e+03	-3.9e+03	-2.67e+03	-3.30e+03	-3.55e+03	-2.92e+03	-3.45e+03
		Std	158.2583	426.9692	147.8735	338.2298	333.8527	583.9779	325.5285	273.7657
	D =50	Avg	-5.8e+03	-1.06e+04	-8.1e+03	-8.73e+03	-1.33e+04	-1.74e+04	-1.25e+04	-1.19e+04
		Std	413.0177	1.63e+03	-1.1e+04	1.50e+03	1.77e+03	3.14e+03	928.4356	1.13e+03
	D=100	Avg	-8.1e+03	-1.63e+04	593.0749	-1.58e+04	-2.28e+04	-3.68e+04	-2.38e+04	-2.01e+04
		Std	526.2818	2.99e+03	696.1978	3.13e+03	2.24e+03	5.64e+03	1.52e+03	3.29e+03
F24	D = 10	Avg	-1.8013	-1.7746	-1.7935	-1.8013	-1.8013	-1.7479	-1.7746	-1.8013
		Std	1.91e-08	0.1463	0.0079	1.66e-06	9.03e-16	0.2033	0.1463	9.03e-16
	D = 50	Avg	-1.8013	-1.7746	-1.7943	-1.7746	-1.8013	-1.7746	-1.8013	-1.8013
		Std	2.72e-08	0.1463	0.0060	0.1463	9.03e-16	0.1463	3.49e-07	9.03e-16
	D=100	Avg	-1.8013	-1.7817	-1.7958	-1.7746	-1.8013	-1.7479	-1.7746	-1.8013
		Std	3.26e-08	0.1072	0.0039	0.1463	9.03e-16	0.2033	0.1463	9.03e-16
F25	D = 10	Avg	-3.6970	-4.3171	-3.3180	-4.3498	-4.4160	-3.4907	-3.9674	-4.5720
		Std	0.2948	0.4314	0.3025	0.4685	0.2741	0.5416	0.6366	0.0774
	D = 50	Avg	-3.6319	-4.2781	-3.3130	-4.2289	-4.4114	-3.7487	-3.9331	-4.5849
		Std	0.2258	0.3353	0.3120	0.5014	0.2605	0.6431	0.5849	0.0914
	D=100	Avg	-3.6354	-4.2311	-3.3863	-4.3154	-4.2564	-3.6108	-4.1058	-4.5543
		Std	0.2047	0.4594	0.3419	0.4272	0.3828	0.5729	0.4528	0.1646

REFERENCES

[1] E. H. Houssein, D. A. Abdelkareem, M. M. Emam, M. A. Hameed, and M. Younan, "An efficient image segmentation method for skin cancer imaging using improved golden jackal optimization algorithm," *Comput. Biol. Med.*, vol. 149, Oct. 2022, Art. no. 106075, doi: 10.1016/j.compbiomed.2022.106075.

[2] X. Yang, R. Wang, D. Zhao, F. Yu, A. A. Heidari, Z. Xu, H. Chen, A. D. Algarni, H. Elmannai, and S. Xu, "Multi-level threshold segmentation framework for breast cancer images using enhanced differential evolution," *Biomed. Signal Process. Control*, vol. 80, Feb. 2023, Art. no. 104373, doi: 10.1016/j.bspc.2022.104373.

[3] S. Agrawal, R. Panda, P. Choudhury, and A. Abraham, "Dominant color component and adaptive whale optimization algorithm for multilevel thresholding of color images," *Knowl.-Based Syst.*, vol. 240, Mar. 2022, Art. no. 108172, doi: 10.1016/j.knosys.2022.108172.

[4] T. Yigit and H. Celik, "Speed controlling of the PEM fuel cell powered BLDC motor with FOPI optimized by MSA," *Int. J. Hydrogen Energy*, vol. 45, no. 60, pp. 35097–35107, Dec. 2020, doi: 10.1016/j.ijhydene.2020.04.091.

[5] Y. Olmez, G. O. Koca, and Z. H. Akpolat, "Clonal selection algorithm based control for two-wheeled self-balancing mobile robot," *Simul. Model. Pract. Theory*, vol. 118, Jul. 2022, Art. no. 102552, doi: 10.1016/j.simpat.2022.102552.

[6] Ö. Inik, "CNN hyper-parameter optimization for environmental sound classification," *Appl. Acoust.*, vol. 202, Jan. 2023, Art. no. 109168, doi: 10.1016/j.apacoust.2022.109168.

[7] R. Mohakud and R. Dash, "Skin cancer image segmentation utilizing a novel EN-GWO based hyper-parameter optimized FCEDN," *J. King Saud Univ. Comput. Inf. Sci.*, vol. 34, no. 10, pp. 9889–9904, Nov. 2022, doi: 10.1016/j.jksuci.2021.12.018.

[8] M. Wang, Y. Liang, Z. Hu, S. Chen, B. Shi, A. A. Heidari, Q. Zhang, H. Chen, and X. Chen, "Lupus nephritis diagnosis using enhanced moth flame algorithm with support vector machines," *Comput. Biol. Med.*, vol. 145, Jun. 2022, Art. no. 105435, doi: 10.1016/j.compbiomed.2022.105435.

[9] S. Yadav, R. Yadav, A. Kumar, and M. Kumar, "A novel approach for optimal design of digital FIR filter using grasshopper optimization algorithm," *ISA Trans.*, vol. 108, pp. 196–206, Feb. 2021, doi: 10.1016/j.isatra.2020.08.032.

[10] I. H. Hassan, A. Mohammed, and Y. S. Ali, "Metaheuristic algorithms in text clustering," in *Comprehensive Metaheuristics*, S. Mirjalili and A. H. Gandomi, Eds. New York, NY, USA: Academic, 2023, pp. 131–152.

[11] T. Dokeroglu, A. Deniz, and H. E. Kiziloz, "A comprehensive survey on recent metaheuristics for feature selection," *Neurocomputing*, vol. 494, pp. 269–296, Jul. 2022, doi: 10.1016/j.neucom.2022.04.083.

[12] Y. Olmez, A. Sengur, G. O. Koca, and R. V. Rao, "An adaptive multilevel thresholding method with chaotically-enhanced rao algorithm," *Multimedia Tools Appl.*, vol. 82, no. 8, pp. 12351–12377, Mar. 2023, doi: 10.1007/s11042-022-13671-9.

[13] R. Kurban, A. Durmus, and E. Karakose, "A comparison of novel metaheuristic algorithms on color aerial image multilevel thresholding," *Eng. Appl. Artif. Intell.*, vol. 105, Oct. 2021, Art. no. 104410, doi: 10.1016/j.engappai.2021.104410.

[14] M. Swain, T. T. Tripathy, R. Panda, S. Agrawal, and A. Abraham, "Differential exponential entropy-based multilevel threshold selection methodology for colour satellite images using equilibrium-cuckoo search optimizer," *Eng. Appl. Artif. Intell.*, vol. 109, Mar. 2022, Art. no. 104599, doi: 10.1016/j.engappai.2021.104599.

[15] L. Ren, D. Zhao, X. Zhao, W. Chen, L. Li, T. Wu, G. Liang, Z. Cai, and S. Xu, "Multi-level thresholding segmentation for pathological images: Optimal performance design of a new modified differential evolution," *Comput. Biol. Med.*, vol. 148, Sep. 2022, Art. no. 105910, doi: 10.1016/j.compbiomed.2022.105910.

[16] W. Zhu, L. Liu, F. Kuang, L. Li, S. Xu, and Y. Liang, "An efficient multi-threshold image segmentation for skin cancer using boosting whale optimizer," *Comput. Biol. Med.*, vol. 151, Dec. 2022, Art. no. 106227, doi: 10.1016/j.compbiomed.2022.106227.

[17] K. M. Hosny, A. M. Khalid, H. M. Hamza, and S. Mirjalili, "Multilevel segmentation of 2D and volumetric medical images using hybrid coronavirus optimization algorithm," *Comput. Biol. Med.*, vol. 150, Nov. 2022, Art. no. 106003, doi: 10.1016/j.compbiomed.2022.106003.

[18] B. Jena, M. K. Naik, R. Panda, and A. Abraham, "Maximum 3D Tsallis entropy based multilevel thresholding of brain MR image using attacking manta ray foraging optimization," *Eng. Appl. Artif. Intell.*, vol. 103, Aug. 2021, Art. no. 104293, doi: 10.1016/j.engappai.2021.104293.

[19] X. Chen, H. Huang, A. A. Heidari, C. Sun, Y. Lv, W. Gui, G. Liang, Z. Gu, H. Chen, C. Li, and P. Chen, "An efficient multilevel thresholding image segmentation method based on the slime mould algorithm with bee foraging mechanism: A real case with lupus nephritis images," *Comput. Biol. Med.*, vol. 142, Mar. 2022, Art. no. 105179, doi: 10.1016/j.compbiomed.2021.105179.

[20] A. Kumar, A. Kumar, A. Vishwakarma, and G. K. Singh, "Multilevel thresholding for crop image segmentation based on recursive minimum cross entropy using a swarm-based technique," *Comput. Electron. Agricult.*, vol. 203, Dec. 2022, Art. no. 107488, doi: 10.1016/j.compag.2022.107488.

[21] J. Wang, J. Bei, H. Song, H. Zhang, and P. Zhang, "A whale optimization algorithm with combined mutation and removing similarity for global optimization and multilevel thresholding image segmentation," *Appl. Soft Comput.*, vol. 137, Apr. 2023, Art. no. 110130, doi: 10.1016/j.asoc.2023.110130.

[22] Y. Ölmez, A. Sengur, and G. O. Koca, "Multilevel thresholding with metaheuristic methods," *J. Fac. Eng. Archit. Gazi Univ.*, vol. 36, no. 1, pp. 213–224, Dec. 2020, doi: 10.17341/gazimmfd.727811.

[23] H. Moazen, S. Molaei, L. Farzinvash, and M. Sabaei, "PSO-ELPM:PSO with elite learning, enhanced parameter updating, and exponential mutation operator," *Inf. Sci.*, vol. 628, pp. 70–91, May 2023, doi: 10.1016/j.ins.2023.01.103.

[24] W. Zhao, L. Wang, and S. Mirjalili, "Artificial hummingbird algorithm: A new bio-inspired optimizer with its engineering applications," *Comput. Methods Appl. Mech. Eng.*, vol. 388, Jan. 2022, Art. no. 114194, doi: 10.1016/j.cma.2021.114194.

[25] C. Zhong, G. Li, and Z. Meng, "Beluga whale optimization: A novel nature-inspired metaheuristic algorithm," *Knowl.-Based Syst.*, vol. 251, Sep. 2022, Art. no. 109215, doi: 10.1016/j.knosys.2022.109215.

[26] L. Abualigah, A. Diabat, S. Mirjalili, M. Abd Elaziz, and A. H. Gandomi, "The arithmetic optimization algorithm," *Comput. Methods Appl. Mech. Eng.*, vol. 376, Apr. 2021, Art. no. 113609, doi: 10.1016/j.cma.2020.113609.

[27] S. Mirjalili, S. M. Mirjalili, and A. Lewis, "Grey wolf optimizer," *Adv. Eng. Softw.*, vol. 69, pp. 46–61, Mar. 2014, doi: 10.1016/j.advengsoft.2013.12.007.

[28] S. Mirjalili, "Moth-flame optimization algorithm: A novel nature-inspired heuristic paradigm," *Knowl.-Based Syst.*, vol. 89, pp. 228–249, Nov. 2015, doi: 10.1016/j.knosys.2015.07.006.

[29] S. Mirjalili and A. Lewis, "The whale optimization algorithm," *Adv. Eng. Softw.*, vol. 95, pp. 51–67, May 2016, doi: 10.1016/j.advengsoft.2016.01.008.

[30] S. Mirjalili, S. M. Mirjalili, and A. Hatamlou, "Multi-verse optimizer: A nature-inspired algorithm for global optimization," *Neural Comput. Appl.*, vol. 27, no. 2, pp. 495–513, Feb. 2016, doi: 10.1007/s00521-015-1870-7.

[31] R. V. Rao, V. J. Savsani, and D. P. Vakharia, "Teaching–learning-based optimization: A novel method for constrained mechanical design optimization problems," *Comput.-Aided Des.*, vol. 43, no. 3, pp. 303–315, Mar. 2011, doi: 10.1016/j.cad.2010.12.015.

[32] c. S. Varnan, K. J. A. Jagan, D. Jyoti, and D. S. Rao, "Image quality assessment techniques PN spatial domain," *Int. J. Comput. Sci. Technol.*, vol. 2, pp. 177–184, Jan. 2011.

[33] L. Zhang, L. Zhang, X. Mou, and D. Zhang, "FSIM: A feature similarity index for image quality assessment," *IEEE Trans. Image Process.*, vol. 20, no. 8, pp. 2378–2386, Aug. 2011.

[34] Z. Wang, A. C. Bovik, H. R. Sheikh, and E. P. Simoncelli, "Image quality assessment: From error visibility to structural similarity," *IEEE Trans. Image Process.*, vol. 13, no. 4, pp. 600–612, Apr. 2004.

[35] D. Karaboga and B. Akay, "A comparative study of artificial bee colony algorithm," *Appl. Math. Comput.*, vol. 214, no. 1, pp. 108–132, Aug. 2009, doi: 10.1016/j.amc.2009.03.090.

YAGMUR OLMEZ received the B.Sc. and M.Sc. degrees in mechatronics engineering from the Institute of Science, Firat University, Elâziğ, Turkey, in 2015 and 2018, respectively. She is currently a Research Assistant of mechatronics engineering with the Faculty of Technology, Firat University. Her research interests include image processing, metaheuristic algorithms, artificial intelligence, system modeling, and control techniques.

GONCA OZMEN KOCA was born in Elâziğ, in 1980. She received the master's degree from the Department of Electronics and Computer Education, Institute of Science, Firat University, in 2005, and the Ph.D. degree from the Electric and Electronic Engineering Department, Firat University. She is currently an Associate Professor with the Control Division, Mechatronics Engineering Department, Technology Faculty, Firat University. Her research interests include control systems, path planning, biomimetic systems, intelligent control techniques, and optimization methods.

ABDULKADIR SENGÜR received the B.Sc. degree in electronics and computers education, the M.Sc. degree in electronics education, and the Ph.D. degree in electrical and electronics engineering from Firat University, Turkey, in 1999, 2003, and 2006, respectively. He was a Research Assistant with the Technical Education Faculty, Firat University, in February 2001. He is currently a Professor with the Technology Faculty, Firat University. His research interests include signal processing, image segmentation, pattern recognition, medical image processing, and computer vision and deep learning.

U. RANJENDRA ACHARYA (Senior Member, IEEE) received the Ph.D., D.Eng., and D.Sc. degrees. He is currently a Professor with the University of Southern Queensland, Australia; a Distinguished Professor with the International Research Organization for Advanced Science and Technology, Kumamoto University, Japan; and an Adjunct Professor with the University of Malaya, Malaysia, and Asia University, Taiwan. His funded research has accrued cumulative grants exceeding six million Singapore dollars. He has authored over 500 publications, including 345 in refereed international journals, 42 in international conference proceedings, and 17 books. He has received more than 74,000 citations on Google Scholar (with an H-index of 136). His research interests include biomedical imaging and signal processing, data mining, and visualization, and the applications of biophysics for better healthcare design and delivery. He has been ranked in the top 1% of the highly cited researchers for the last seven consecutive years (2016–2022) in computer science, according to the Essential Science Indicators of Thomson. He is on the editorial boards of many journals and has served as a guest editor on several AI-related issues.

HASAN MIR (Senior Member, IEEE) received the B.S. (cum laude), M.S., and Ph.D. degrees in electrical engineering from the University of Washington, Seattle, WA, USA, in 2000, 2001, and 2005, respectively. From 2005 to 2009, he was with the Air Defense Technology Group, Lincoln Laboratory, Massachusetts Institute of Technology, Lexington, MA, USA. Since 2009, he has been with the Department of Electrical Engineering, American University of Sharjah, Sharjah, United Arab Emirates, where he is currently an Associate Professor.